



## Research paper

# Antiproliferative, DNA intercalation and redox cycling activities of dioxonaphtho[2,3-d]imidazolium analogs of YM155: A structure–activity relationship study



Si-Han Sherman Ho<sup>a</sup>, Mei-Yi Sim<sup>b</sup>, Wei-Loong Sherman Yee<sup>a</sup>, Tianming Yang<sup>a</sup>, Shyi-Peng John Yuen<sup>b</sup>, Mei-Lin Go<sup>a,\*</sup>

<sup>a</sup> Department of Pharmacy, National University of Singapore, 18 Science Drive 4, 117543, Republic of Singapore

<sup>b</sup> Department of Urology, Singapore General Hospital, 20 College Road, 169856, Republic of Singapore

## ARTICLE INFO

## Article history:

Received 18 May 2015

Received in revised form

17 August 2015

Accepted 21 September 2015

Available online 25 September 2015

## Keywords:

YM155

DNA intercalation

Redox cycling

Cell viability

Survivin suppressant

Apoptosis

## ABSTRACT

The anticancer agent YM155 is widely investigated as a specific survivin suppressant. More recently, YM155 was found to induce DNA damage and this has raised doubts as to whether survivin is its primary target. In an effort to assess the contribution of DNA damage to the anticancer activity of YM155, several analogs were prepared and evaluated for antiproliferative activity on malignant cells, participation in DNA intercalation and free radical generation by redox cycling. The intact positively charged scaffold was found to be essential for antiproliferative activity and intercalation but was less critical for redox cycling where the minimal requirement was a pared down bicyclic quinone. Side chain requirements at the N<sup>1</sup> and N<sup>3</sup> positions of the scaffold were more alike for redox cycling and intercalation than antiproliferative activity, underscoring yet again, the limited structural overlaps for these activities. Furthermore, antiproliferative activities were poorly correlated to DNA intercalation and redox cycling. Potent antiproliferative activity (IC<sub>50</sub> 9–23 nM), exceeding that of YM155, was found for a minimally substituted methyl analog **AB7**. Like YM155 and other dioxonaphthoimidazoliums, **AB7** was a modest DNA intercalator but with weak redox cycling activity. Thus, the capacity of this scaffold to inflict direct DNA damage leading to cell death may not be significant and YM155 should not be routinely classified as a DNA damaging agent.

© 2015 Elsevier Masson SAS. All rights reserved.

## 1. Introduction

Survivin is an anti-apoptotic protein that belongs to the family of Inhibitor of Apoptosis Proteins (IAP). It is selectively expressed in a plethora of cancers [1–7] but undetectable in most terminally differentiated adult tissues [8]. Clinically, survivin expression is correlated to several cancer-related events such as metastatic

spread, tumor invasiveness and poor prognosis arising from chemoresistance [9,10]. Survivin is a nodal molecule with global effects on multiple signaling pathways in cancer cells. Thus, it is widely regarded as an attractive therapeutic target in cancer [3,4,11]. To date, only a few small molecules have been proposed as specific inhibitors of survivin (Fig. 1) [12–14]. Of these, the dioxonaphtho [2,3-d]imidazolium YM155 (sepantronium bromide) is the most widely investigated and the only member to be advanced to clinical trials [15–17].

YM155 blocks the transcription of the survivin gene by intercepting the binding of transcription factors ILF3/NF110 and SP1 to the survivin promoter [18,19]. It also induces dissociation of the ILF3-p54nrb complex which positively regulates survivin expression [20]. However, there is mounting evidence that YM155-induced effects are not solely due to the inhibition of survivin [21]. YM155 reduced the transcription and expression of MCL1, another anti-apoptotic protein, in various tumors [22]. It also suppressed EGFR signaling, in part by inducing the proteasomal

**Abbreviations:** p54<sup>nrb</sup>, nuclear RNA-binding protein; ILF3/NF110, interleukin enhancer binding factor 3/nuclear factor 110; SP1, specificity factor 1; STAT3, signal transducer and activator of transcription 3; PI3K, phosphoinositide 3-kinase; KAP1, KRAB-associated protein 1; MCL1, myeloid cell leukemia 1; ERK, extracellular signal-regulated kinase; GAPDH, glyceraldehyde 3-phosphate dehydrogenase; H<sub>2</sub>DCF, 2',7' dichlorodihydrofluorescein; MTT, 3-(4,5-dimethylthiazol-2-yl)-2,5-diphenyltetrazolium bromide; SLC35F2, solute carrier family 35 member F2; HES1, Hairy and Enhancer of split-1; PER, period circadian protein.

\* Corresponding author.

E-mail addresses: [phagoml@nus.edu.sg](mailto:phagoml@nus.edu.sg), [meilin.go@nus.edu.sg](mailto:meilin.go@nus.edu.sg) (M.-L. Go).

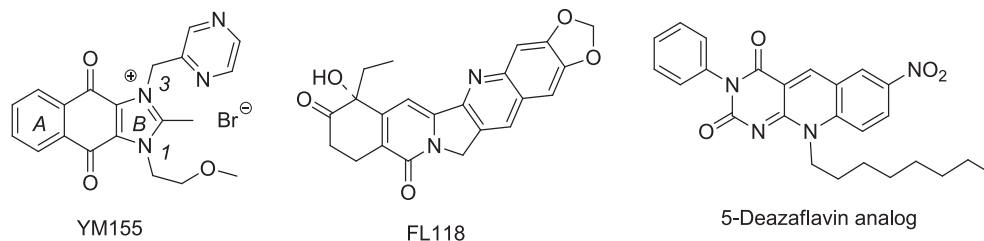


Fig. 1. Small molecules with anticancer activities reportedly linked to suppression of survivin.

degradation of EGFR [23]. The levels of other cancer related molecules like PI3K, ERK, STAT3, securin were also diminished in the presence of YM155 [23,24]. A transcriptome analysis of Wilms' tumor cells treated with YM155 revealed down-regulation of several other genes besides survivin as well as the up-regulation of the pro-apoptotic genes caspase 9 and DIABLO [25]. More critically, reports have surfaced that YM155 increased levels of the DNA damage markers  $\gamma$ H2AX and phosphorylated KAP1 in malignant cells [26,27]. This has led to the proposal that YM155 acts primarily by inducing DNA damage and that any effect on survivin is a secondary event caused by the general deactivation of gene expression brought about by DNA damage [26].

For an agent to induce DNA damage, it must necessarily interact reversibly or irreversibly with DNA [27]. Irreversible binding would involve alkylation of the DNA bases while reversible binding may occur by charge–charge interactions with the phosphate backbone, interactions with the edges of base pairs in either the major or minor groove or via insertion of the agent between base pairs of the double helix (intercalation). Reversible binding is followed by a cascade of events culminating in DNA damage. These events may involve topoisomerase-induced DNA damage, inhibition of DNA polymerase activity or the generation of free radicals that cause DNA strand breaks. Structurally, YM155 is an improvable alkylating agent as it lacks features associated with a reactive electrophilic center. On the other hand, the positively charged planar scaffold of YM155 would favor intercalation with DNA. Intercalation followed by disruption of DNA winding by topoisomerases is unlikely as YM155 was not found to inhibit topoisomerase I [28]. On the other hand, there is a greater likelihood of free radical induced DNA damage as the embedded quinone moiety in YM155 is an established pharmacophore for redox cycling [29] and free radicals generated during the quinone to semiquinone interconversion could readily initiate DNA strand breaks.

To date, little is known of the structural features of YM155 that are critical for DNA binding or redox cycling. In fact, the structure–activity relationship (SAR) for anticancer activity of the dioxonaphthoimidazolium scaffold has not been clearly defined even though nearly 250 YM155 analogs modified at the benzene ring A and imidazolium ring B were disclosed in the patent on YM155 (Fig. 1) [12]. Antiproliferative activities ( $IC_{50}$ ) on HeLaS3 and melanoma A375 cells were cited to be 1  $\mu$ M or less for the entire series but without details on assigned activities or structure-activity trends [12]. The closest reference, aside from the patent, identified 1-ethyl-2-methylnaphth[2,3-d]imidazole-4,9-dione (**1**) as a cytotoxic candidate with a mean  $GI_{50}$  of 2.3  $\mu$ M on tumor cell lines of the NCI panel [30]. Notably, two intermediates (**2**, **3**) involved in the synthesis of **1** and related compounds had comparable activities (Fig. 2). In view of the recent claims of DNA damage by YM155, a comprehensive understanding of the key features of the scaffold that promote DNA interaction, redox cycling and anti-cancer activity would serve to define the contribution of the DNA damage response to the antiproliferative activity of YM155. Common or overlapping structural features would strengthen the notion that

YM155 acts primarily as a DNA damage agent. Greater certainty in the molecular target of YM155 would aid in the selection of patients and drugs to be used with it in combination chemotherapy [31]. To this end, a focus library of dioxonaphthoimidazolium analogs was prepared as part of the structure–activity relationship (SAR) exploration of YM155. These compounds were screened for anti-proliferative activities on two malignant cell types and evaluated by appropriate assays for the detection of DNA intercalation and redox cycling by reactive oxygen species.

## 2. Chemistry

Four series of YM155 analogs comprising 53 compounds were synthesized and evaluated on clear cell renal cell carcinoma (ccRCC) and non-small cell lung carcinoma (NSCLC) cell lines (Fig. 3). Series A compounds were modified at the N<sup>3</sup> pyrazin-2'-ylmethyl side chain of YM155 with no change at the N<sup>1</sup> 2'-methoxyethyl side chain. Conversely, series B involved changes to the N<sup>1</sup> 2'-methoxyethyl arm while retaining the N<sup>3</sup> pyrazin-2'-ylmethyl side chain. In each case, modifications were made to delineate the importance of the functionality that was being altered. Hence in series A, we replaced the pyrazine ring with benzene, cyclohexane, five-membered heteroaromatics (thiophene, imidazole), other azines (pyridine, pyrimidine, pyridazine), alkyl side chains as well as varying the length of the methylene linker between the ring and the scaffold. In series B, the 2'-methoxyethyl side chain was replaced by various alkyl homologs, aromatic rings (benzyl, pyrazinylmethyl) and hydroxyl or amino functionalities in place of methoxy. Series C involved changes to the dioxonaphthoimidazolium scaffold of YM155. These included removing the positive charge from the scaffold and stepwise reduction of the tricyclic scaffold to a single ring. Series AB incorporated functionalities that were associated with “optimal” anti-proliferative activities from series A and B.

The synthesis of compounds in series A, B and AB followed the general method described in the literature [12]. As shown in Scheme 1, nucleophilic displacement of chlorine in 2,3-dichloro-1,4-naphthoquinone was effected by a primary amine in the presence of triethylamine to yield compounds **4–15**. The amino nitrogen was then acetylated to give *N*-acetylamides **16–27**, followed by displacement of the second chlorine by another primary amine to give compounds **28–70**. Finally, ring closure was effected by hydrobromic acid to give the final compounds (Scheme 1). In this way, the compounds in series A, B and AB were successfully prepared in yields ranging from 6 to 97%. A different route was applied for the synthesis of **A5-1**. The *N*-acetylamide **16** was subjected to a modified Buchwald–Hartwig coupling reaction with 2-aminopyrazine to give **71**, followed by ring closure in the presence of hydrobromic acid (Scheme 2).

Scheme 1 also applied to the series C compounds **C1-1**, **C1-2** and **C2-3** with some modifications. To obtain **C1-1**, propionic anhydride was used in place of acetic anhydride for the acylation of **4**. The resulting *N*-propionate **72** was reacted with pyrazin-2-

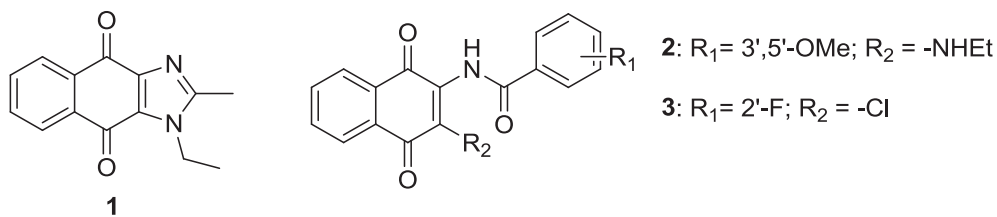


Fig. 2. Naphtho[2,3-d]imidazole-4,9-dione **1** and intermediates (**2,3**) with anticancer activity on NCI cancer cell lines.

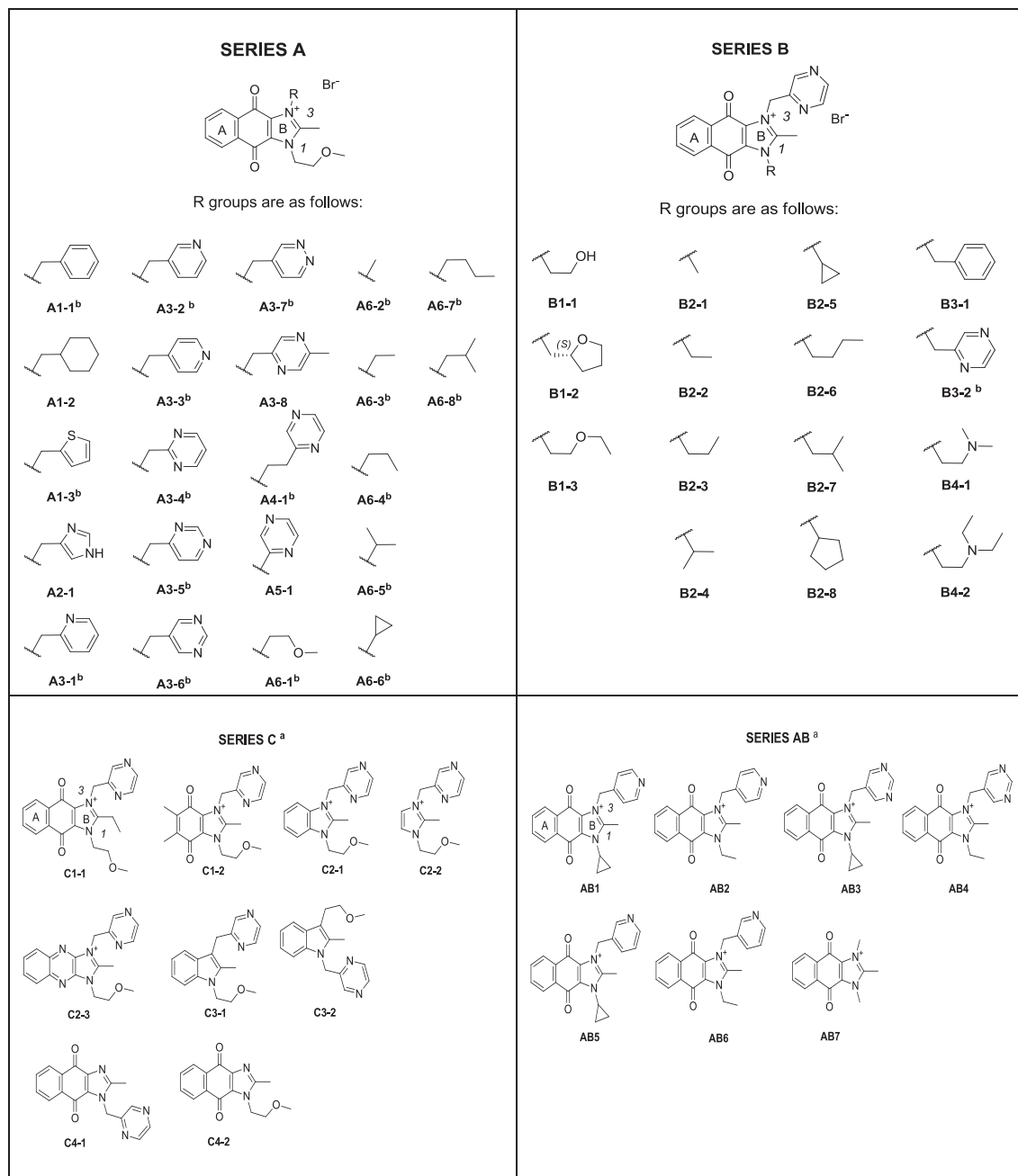
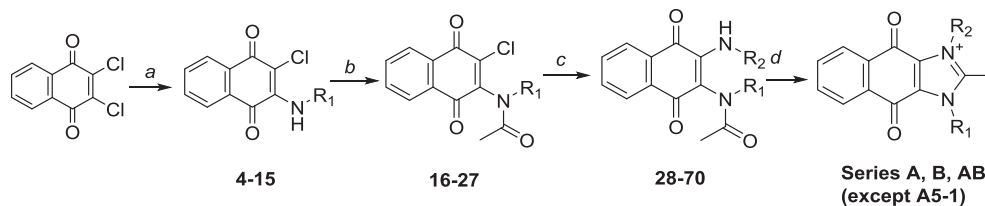


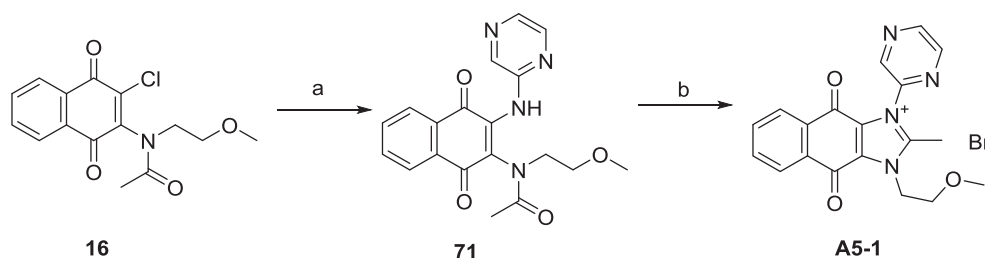
Fig. 3. Structures of synthesized compounds. <sup>a</sup>Positively charged analogs in series C and series AB were synthesized as bromides. <sup>b</sup>Have been reported in literature [12]. The remaining 34 analogs are novel.

ylmethanamine to afford **73** which was then cyclized to **C1-1**. In the case of **C1-2** and **C2-3**, the same sequence of reactions were followed starting from 2,3-dichloro-5,6-dimethyl-1,4-

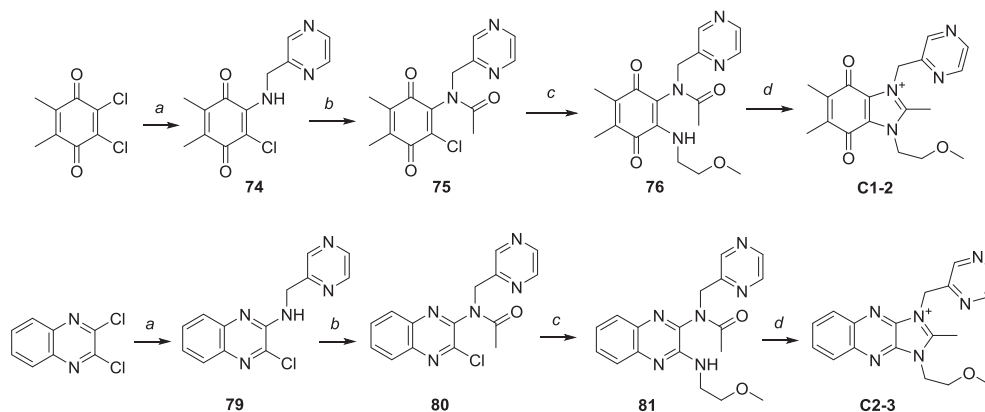
benzoquinone and 2,3-dichloroquinoxaline respectively, except that the initial displacement of chlorine was effected by pyrazin-2-ylmethanamine and not 2-methoxyethanamine (Scheme 3).



**Scheme 1.** Reagents and conditions: (a) R<sub>1</sub>-amines, EtOH, r.t., 18 h; (b) acetic anhydride, conc. H<sub>2</sub>SO<sub>4</sub>, r.t., 1.5 h; (c) R<sub>2</sub>-amines, toluene, 45 °C, 4 h; (d) 48% HBr (aq), EtOH + EtOAc, 45 °C, 4 h to r.t., overnight.



**Scheme 2.** Reagents and conditions: (a) 2-Aminopyrazine, Pd(dba)<sub>2</sub>, BINAP, t-BuOK, toluene, 60 °C, 5 h; (b) 48% HBr (aq), EtOH + EtOAc, 45 °C, 4 h to r.t., overnight.



**Scheme 3.** Reagents and conditions: (a) Pyrazin-2-ylmethylamine, triethylamine; (b) Acetic anhydride, conc. H<sub>2</sub>SO<sub>4</sub>; (c) 2-Methoxyethylamine, toluene; (d) 48% HBr (aq), EtOH + EtOAc, 45 °C, 4 h to r.t., overnight.

The benzimidazolium **C2-1** and imidazolium **C2-2** were synthesized by *N*-alkylation with 2-methoxyethyl bromide to give **77** and **78** respectively, followed by quaternization of the azomethine nitrogen with 2-bromomethylpyrazine [32,33]. Scheme 4 outlines the synthesis of **C2-1**, which also applies to **C2-2**.

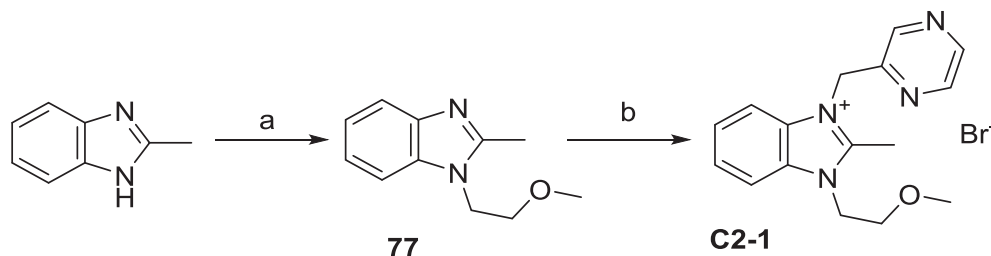
Scheme 5 outlines the syntheses of the isomeric indoles **C3-1** and **C3-2**. 2-Methylindole was reacted with pyrazin-2-carbaldehyde in the presence of triethylsilane and trifluoroacetic acid to give **82** [32] which was then *N*-alkylated in the presence of KOH in DMSO to afford **C3-1** [33]. In the case of **C3-2**, 2-methylindole was reacted at the indole nitrogen with methyl magnesium bromide, followed by electrophilic substitution at C<sup>3</sup> with 2-methoxyethyl bromide [33]. The pyrazinylmethyl side chain was then introduced at the indole N in the usual way [32].

The synthesis of **C4-1** and **C4-2** was adapted from Scheme 1. Nucleophilic displacement of chlorine in 2,3-dichloro-1,4-naphthoquinone was effected by concentrated ammonia to give **84**, followed by acetylation by acetic anhydride to give **85**. Nucleophilic displacement of the second chlorine by 2-methoxyethylamine or pyrazin-2-ylmethylamine gave **86** and **87** respectively. Finally, ring closure using hydrobromic acid yielded **C4-1** and **C4-2** respectively (Scheme 6).

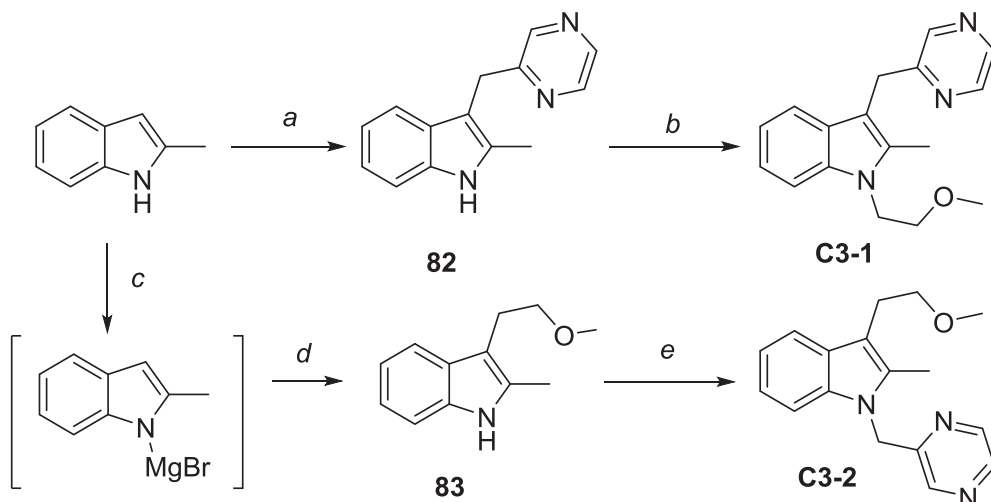
### 3. Results

#### 3.1. Cell-based antiproliferative activities

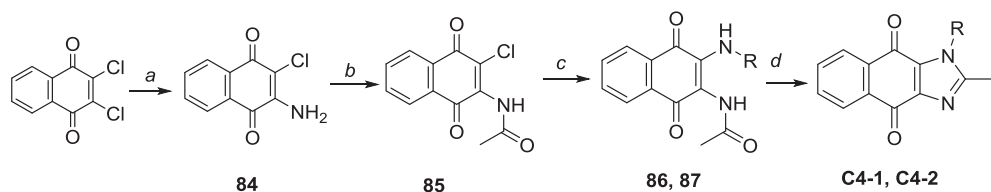
The synthesized compounds were evaluated for their anti-proliferative effects on the clear cell renal cell carcinoma (ccRCC) cell lines (RCC786-0, RCC4/VA), the non-small cell lung carcinoma (NSCLC) cell lines (H1299, H1666) and the non-malignant human lung fibroblast IMR-90 cells. RCC786-0 and RCC4/VA are deficient in the tumor suppressor von Hippel-Lindau (VHL) gene, a genetic aberration that is commonly encountered in ccRCC. Suppression of the VHL gene is observed in up to 91% of sporadic ccRCC cases [34]. H1299 cells are p53-null unlike H1666 cells which are p53 positive. The antiproliferative activities of the test compounds were expressed in terms of IC<sub>50</sub> which is the concentration required to reduce cell viability to 50% of levels observed in untreated cells under similar experimental conditions. The median IC<sub>50</sub> values were calculated for each cell line and found to be 113 nM (H1666), 192 nM (H1299), 262 nM (RCC786-0) and 633 nM (RCC4/VA). Differences in the sensitivities of the different cell lines were no more than 6-fold and ranking of compounds in terms of antiproliferative potency was broadly consistent within each cell line. For example,



**Scheme 4.** Reagents and conditions: (a) 2-methoxyethyl bromide, KOH, DMSO, r.t., 1.5 h; (b) 2-bromomethylpyrazine, CH<sub>3</sub>CN, 80 °C, 24 h.



**Scheme 5.** Reagents and conditions: (a) Pyrazin-2-carbaldehyde, Et<sub>3</sub>SiH, TFA, DCM, 0 °C, 1 h; (b) 2-Methoxyethyl bromide, KOH, DMSO, r.t., 1.5 h; (c) MeMgBr, dry toluene, DCM, 0 °C, 30 min; (d) 2-Methoxyethyl bromide, 0 °C → 40 °C, 24 h; (e) 2-Bromomethylpyrazine, KOH, DMSO, r.t., 30 min.



**Scheme 6.** Reagents and conditions: (a) NH<sub>3</sub> in MeOH, EtOH, 35 °C, 3 h; (b) Acetic anhydride, conc. H<sub>2</sub>SO<sub>4</sub>, r.t., 1.5 h; (c) 2-Methoxyethylamine/pyrazin-2-ylmethylamine, triethylamine, toluene + EtOH, 45 °C, 1 h; (d) 48% HBr (aq), 2 drops of 2 M NaOH(aq), EtOH, 50 °C, 1 h.

**A5-1** had the weakest antiproliferative activity on all cells while the most potent compounds were either **A3-3** or **AB7**. This trend was also reflected in the Spearman correlation coefficients ( $\rho$ ) derived from pair-wise comparisons of IC<sub>50</sub> values from the four cell lines.  $\rho$  values exceeded 0.85, indicating a strong monotonic relationship between the IC<sub>50</sub> values (Supporting Information Table S1). Hence the SAR deduced from one cell line should largely apply to other cell lines. In the following paragraphs, SAR is discussed with reference to H1666 cells. Table 1 lists the IC<sub>50</sub> values derived from the highly susceptible H1666 cells. Values for the other cell lines are given in Supporting Information (Table S2).

We first considered the series C compounds to deduce the importance of the dioxonaphthoimidazolium scaffold. YM155 had an IC<sub>50</sub> of 13.7 nM on H1666 cells and removal of the benzene ring to give the dioxodihydrobenzoimidazolium **C1-2** (IC<sub>50</sub> 584 nM) resulted in a modest loss of activity. On the other hand, omitting the quinone moiety to give the benzoimidazolium **C2-1** completely abolished activity (IC<sub>50</sub> > 100  $\mu$ M) and the same was true when the scaffold was trimmed down to a solitary imidazolium ring (**C2-2**).

The importance of the quinone moiety was again emphasized by the negligible activity of the quinoxalinoimidazolium analog **C2-3** (IC<sub>50</sub> > 100  $\mu$ M). Loss of the permanent positive charge on the scaffold as seen in the dioxonaphthoimidazoles (**C4-1**, **C4-2**) and naphthoquinone which is YM155 without the positively charged imidazolium ring, likewise reduced IC<sub>50</sub> but to a lesser degree (IC<sub>50</sub> 10–20  $\mu$ M) as compared to the omission of the quinone. Broadly, these results support the view that loss of the quinone from the tricyclic scaffold was the most detrimental, followed by omission of the positive charged imidazolium (**C4-1**, **C4-2**, naphthoquinone) while the least disruptive modification was the removal of the distal benzene ring (**C1-2**).

Next, we assessed the importance of the three substituents on the dioxonaphthoimidazolium scaffold of YM155. These were the 2'-methoxyethyl at N<sup>1</sup>, methyl at C<sup>2</sup> and pyrazin-2'-ylmethyl at N<sup>3</sup>. Only one modification was made to the methyl at C<sup>2</sup>, which was extension to its ethyl homolog. The resulting compound (**C1-1**, IC<sub>50</sub> 96 nM) was less active indicating a preference for a sterically small group at this position.

**Table 1**  
Antiproliferative IC<sub>50</sub> values of YM155 and synthesized compounds on non-small cell lung cancer H1666 and non-malignant IMR-90 cells.

Cpd	Antiproliferative IC <sub>50</sub> , μM <sup>a</sup>		
	H1666	IMR-90	Selectivity ratio <sup>b</sup>
YM155	0.0137 ± 0.0009	0.247 ± 0.037	18
A1-1	0.240 ± 0.020	1.16 ± 0.07	4.8
A1-2	0.415 ± 0.029	5.27 ± 0.96	13
A1-3	0.207 ± 0.017	1.45 ± 0.05	7.0
A2-1	0.279 ± 0.027	2.01 ± 0.11	7.2
A3-1	0.231 ± 0.033	2.52 ± 0.11	11
A3-2	0.0404 ± 0.0052	0.611 ± 0.044	15
A3-3	0.0110 ± 0.0007	0.176 ± 0.009	16
A3-4	0.152 ± 0.003	3.18 ± 0.04	21
A3-5	0.00770 ± 0.00070	0.205 ± 0.014	27
A3-6	0.0287 ± 0.0027	0.276 ± 0.027	9.6
A3-7	0.0199 ± 0.0021	0.187 ± 0.012	9.4
A3-8	0.157 ± 0.003	2.00 ± 0.13	13
A4-1	0.859 ± 0.090	2.81 ± 0.52	3.3
A5-1	8.78 ± 0.09	8.82 ± 1.21	1.0
A6-1	0.0728 ± 0.0056	0.743 ± 0.089	10
A6-2	0.0288 ± 0.0054	0.345 ± 0.038	12
A6-3	0.073 ± 0.0035	1.23 ± 0.13	17
A6-4	0.113 ± 0.018	1.72 ± 0.083	15
A6-5	0.224 ± 0.02	3.89 ± 0.29	17
A6-6	0.0559 ± 0.0111	1.16 ± 0.14	21
A6-7	0.15 ± 0.027	2.64 ± 0.54	18
A6-8	0.278 ± 0.056	6.79 ± 0.29	24
B1-1	0.118 ± 0.017	2.48 ± 0.32	21
B1-2	0.758 ± 0.121	9.89 ± 0.17	13
B1-3	0.0377 ± 0.0045	1.43 ± 0.26	38
B2-1	0.0415 ± 0.0081	0.582 ± 0.089	14
B2-2	0.0349 ± 0.0020	0.480 ± 0.022	14
B2-3	0.0405 ± 0.0033	0.565 ± 0.027	14
B2-4	0.152 ± 0.009	1.42 ± 0.15	9.3
B2-5	0.0327 ± 0.0012	0.213 ± 0.020	6.5
B2-6	0.0546 ± 0.0034	1.62 ± 0.14	30
B2-7	0.458 ± 0.025	7.97 ± 0.180	17
B2-8	1.47 ± 0.09	6.58 ± 0.18	4.5
B3-1	1.37 ± 0.09	5.61 ± 0.38	4.1
B3-2	0.450 ± 0.052	3.57 ± 0.71	7.9
B4-1	1.44 ± 0.20	7.42 ± 0.76	5.2
B4-2	1.81 ± 0.15	3.73 ± 0.11	2.1
C1-1	0.0960 ± 0.0127	1.90 ± 0.11	20
C1-2	0.584 ± 0.097	1.36 ± 0.15	2.3
C2-1	>100	>100	N/A <sup>c</sup>
C2-2	>100	>100	N/A <sup>c</sup>
C2-3	>100	>100	N/A <sup>c</sup>
C3-1	>100	>100	N/A <sup>c</sup>
C3-2	>100	>100	N/A <sup>c</sup>
C4-1	22.0 ± 1.5	55.4 ± 4.6	2.5
C4-2	17.9 ± 2.0	73.0 ± 4.5	4.1
AB1	0.0168 ± 0.0017	0.287 ± 0.059	17
AB2	0.0298 ± 0.0032	0.310 ± 0.051	10
AB3	0.0862 ± 0.0070	0.649 ± 0.079	7.5
AB4	0.0613 ± 0.0054	0.440 ± 0.007	7.2
AB5	0.0533 ± 0.0041	0.484 ± 0.064	9.1
AB6	0.0355 ± 0.0049	0.475 ± 0.091	13
AB7	0.00860 ± 0.00030	0.159 ± 0.016	18
d	9.78 ± 0.56	13.3 ± 2.0	1.4



<sup>a</sup> Evaluated by MTT assay, 72 h incubation, 37 °C, 5% CO<sub>2</sub>. Mean ± SD for n = 3 independent determinations.

<sup>b</sup> Mean IC<sub>50</sub> IMR-90/IC<sub>50</sub> H1666.

<sup>c</sup> Not applicable.

<sup>d</sup> Naphthoquinone.

The series A compounds were designed to probe the importance of the pyrazin-2'-ylmethyl side chain at N<sup>3</sup>. The following observations apply. First, extending the side chain to pyrazin-2'-ylethyl (**A4-1**, IC<sub>50</sub> 86 nM) or truncating it to pyrazin-2'-yl (**A5-1**, IC<sub>50</sub> 8.8 μM) reduced activity. Second, replacing pyrazin-2'-ylmethyl

with non-azinylmethyl rings like benzyl (**A1-1**, IC<sub>50</sub> 240 nM), cyclohexylmethyl (**A1-2**, 415 nM), thien-2'-ylmethyl (**A1-3**, IC<sub>50</sub> 207 nM) or imidazol-2'-ylmethyl (**A2-1**, IC<sub>50</sub> 279 nM) adversely affected antiproliferative activity. Third, substituting pyrazine with other azines (pyridine, pyrimidine and pyridazine) was generally well tolerated but for selected regioisomers only. There was a noticeable bias against azines with only ortho-substituted azomethine nitrogens. Thus, among the pyridinylmethyl analogs, the ortho substituted analog (**A3-1**, pyridin-2'-ylmethyl) fared poorly compared to its meta (**A3-2**) and para (**A3-3**) counterparts. This was also true for the pyrimidinylmethyl analogs where the exclusively ortho substituted **A3-4** consistently underperformed when compared to its regioisomers **A3-5** (ortho and para Ns) and **A3-6** (two meta Ns). The apparent preference for the meta- or para regioisomer may reflect the optimal location of the azomethine N for hydrogen bonding. We noted that inserting a methyl at the para position of the pyrazine ring of YM155 reduced activity by 10-fold (**A3-8**, IC<sub>50</sub> 157 nM) which implied that in the absence of a para-azomethine N, it is best to keep that position unoccupied. Even then, the preferred regioisomers (**A3-3**, **A3-5**, **A3-7**) were only equivalent or modestly exceeded YM155 in terms of antiproliferative activity. Lastly, replacing the pyrazinylmethyl side chain with alkyl side chains (**A6-1** to **A6-8**) was an acceptable modification. Seven alkyl side chains were investigated and of these, methyl was the most active on H1666 cells, followed by cyclopropyl, ethyl, propyl, n-butyl, isopropyl and isobutyl in that order. The same sequence of methyl > ethyl > propyl was observed on the other cell lines, corroborating a preference for short alkyl side chains that were not branched or cyclized. Even so, the highly ranked methyl analog **A6-2** (IC<sub>50</sub> 29 nM) was at best comparable to YM155 and the azinylmethyl analogs (**A3-3**, **A3-5**, **A3-7**).

The series B compounds were designed to report on the effects of modifying the 2'-methoxyethyl side chain at N<sup>1</sup> while maintaining methyl and pyrazin-2'-ylmethyl at C<sup>2</sup> and N<sup>3</sup>. Replacing the methoxy with hydroxy resulted in an 8-fold loss in activity whereas homologation to ethoxy caused a smaller 3-fold loss. Embedding the ether functionality in a ring (tetrahydrofurfuryl, **B1-2**) or replacing it with an *N,N*-disubstituted amine (**B4-1**, **B4-2**) pushed IC<sub>50</sub> values to the micromolar range. On the other hand, replacing methoxyethyl with alkyl side chains afforded compounds with surprisingly good activity. The side chains investigated were similar to those in series A (methyl, ethyl, propyl, butyl isopropyl, isobutyl, cyclopropyl). As before, short unbranched side chains were best but with a different rank order of activity (cyclopropyl > ethyl > propyl > methyl > isopropyl > isobutyl) compared to series A. The preeminent position of the cyclopropyl side chain (**B2-5**) was evident in all cells except RCC786-0, where the methyl and ethyl analogs were more active. Interestingly, we noted that **B2-8** bearing the cyclopentyl side chain fared poorly compared to its potent cyclopropyl counterpart **B2-5**. Thus, the more critical requirement appears to be that of a sterically small group at N<sup>1</sup>, regardless of whether it is cyclized or not.

We also explored the feasibility of replacing methoxyethyl with aromatic ring structures, namely benzyl and pyrazin-2'-ylmethyl. The resulting compounds (**B3-1**, **B3-2**) had significantly diminished activities. **B3-2** is noteworthy as it is symmetrically substituted with pyrazinylmethyl moieties at both N<sup>1</sup> and N<sup>3</sup> and is thus comparable to **A6-1** which is symmetrically substituted at the same positions with 2'-methoxyethyl moieties. That **A6-1** (IC<sub>50</sub> 73 nM) was more potent than **B3-2** (IC<sub>50</sub> 450 nM) further underscores the poor tolerance for bulky substituents on the scaffold. Taken together, series B was less promising than series A with only one member, (the cyclopropyl analog **B2-5**) that was marginally more potent than YM155, and only on H1299 cells.

Having identified N<sup>3</sup>-pyridin-4'-ylmethyl and N<sup>1</sup>-cyclopropyl as

the “optimal” substituents at their respective positions, these functionalities were then introduced to the scaffold with the expectation that it would yield more potent compounds. Less optimal substituents (pyridin-3'-ylmethyl, pyrimidin-5'-ylmethyl, methyl, ethyl) were concurrently investigated to validate this approach. In all, seven analogs were synthesized, of which six were derived from permutations of pyridin-4'-ylmethyl, pyridin-3'-ylmethyl or pyrimidin-5'-ylmethyl at N<sup>3</sup> and ethyl or cyclopropyl at N<sup>1</sup>. The last compound **AB7** was substituted at both N<sup>1</sup> and N<sup>3</sup> with methyl. Good activity was found in analogs that have pyridin-4'-ylmethyl at N<sup>3</sup> and cyclopropyl (**AB1**) or ethyl (**AB2**) at N<sup>1</sup>. **AB1** was broadly equivalent to YM155 in terms of IC<sub>50</sub> while **AB2** was marginally less active than YM155. Clearly, this approach of combining optimal substituents onto the scaffold did not work as well as anticipated. Surprisingly, the minimally substituted **AB7** displayed good antiproliferative activity (IC<sub>50</sub> 8.6 nM versus 13.7 nM for YM155) and is the most promising compound identified in this investigation.

To determine if YM155 and the test compounds selectively affected proliferation of malignant cells, we determined their effects on the viability of non-malignant lung fibroblast IMR-90 cells. Selectivity was assessed from the ratio of IC<sub>50</sub> values on IMR-90 versus the malignant cell line. Values ranging from 1 to 38 were obtained for H1666 (Table 1). Higher selectivities (21–38 fold) were found for compounds that had relatively weaker growth inhibitory activities (**A6-6**, **A6-8**, **B1-3**, **B2-6**) whereas YM155 and its most potent analogs (**A3-3**, **A3-5**, **AB1**, **AB7**) had more modest selectivities ranging from 16 to 27-fold. Selectivity ratios for the other cell lines are found in Table S1.

### 3.2. Intercalation with DNA

Next, we assessed the DNA binding affinity of the test compounds by monitoring the displacement of thiazole orange from herring sperm DNA [35,36]. Briefly, thiazole orange intercalates with non-specific DNA sequences in herring sperm DNA with emission of fluorescence. When it is displaced by a competing intercalator, fluorescence is diminished. Here, each compound was tested over a range of concentrations to determine the concentration (DC<sub>50</sub>) at which it reduced the basal fluorescence of thiazole orange (10 μM) by 50%. Strong intercalators would have small DC<sub>50</sub> values and vice versa. Typical dose response curves depicting the displacement of thiazole orange by competing test compounds are provided in Supporting Information (Figure S1).

The DC<sub>50</sub> of YM155 was 20 μM as compared to 2.6 μM for the positive control doxorubicin (Table 2). Since thiazole orange was evaluated at a fixed concentration of 10 μM, this would imply that YM155 had half the binding affinity of thiazole orange for DNA as compared to doxorubicin which had 4 times the DNA binding affinity of thiazole orange. Clearly, the DNA binding affinity of YM155 was significantly weaker than that of doxorubicin.

Some interesting trends in DNA binding affinities were deduced from the DC<sub>50</sub> values in Table 2. First, an intact dioxonaphthoimidazolium scaffold was required. This was clearly seen from the poor binding affinities (DC<sub>50</sub> > 100 μM) of series C compounds that lack the tricyclic scaffold in its entirety. Omission of the quinone (series C compounds except **C1-1**) or the positive charge (**C4-1**, **C4-2**) from the scaffold significantly reduced binding affinity (DC<sub>50</sub> > 100 μM). Naphthoquinone, a bicyclic quinone, was also a weak intercalator. Thus an intact scaffold was critical for DNA intercalation.

Second, for compounds with intact scaffolds, the absence of ring structures at N<sup>1</sup> and N<sup>3</sup> adversely affected binding. Thus we noted that the series A compounds (**A6-1** to **A6-8**) in which the pyrazin-2-ylmethyl side chain was replaced by alkyl side chains had

diminished affinities (DC<sub>50</sub> 32–99 μM). The corollary that compounds bearing ring structures at N<sup>1</sup> and N<sup>3</sup> should be strong binders was indeed found to apply as seen from **B1-2** (13 μM), **B3-1** (14 μM) and **B3-2** (12 μM). Interestingly, series AB consistently yielded good DNA intercalators (DC<sub>50</sub> 12–23 μM). It is noted that the intercalating ability of **AB1–AB6** were closely aligned to that of the corresponding series A analogs. Thus, **AB1** and **AB2** which have in common a pyridin-4'-ylmethyl side chain had DC<sub>50</sub> values that were within the range of **A3-3** which has a similar side chain at N<sup>3</sup>. This was again observed for **AB5**, **AB6** (compared to **A3-2**) and **AB3** (compared to **A3-6**). **AB4** was an outlier, being more potent than **A3-6**. The strong binding affinity of the N<sup>1</sup>, N<sup>3</sup>-dimethyl substituted **AB7** (DC<sub>50</sub> 13 μM) was unusual because the mono-methyl analogs, (**B2-1**, N<sup>1</sup>-methyl, DC<sub>50</sub> 31 μM; **A6-2**, N<sup>3</sup>-methyl, DC<sub>50</sub> 32 μM) were significantly weaker intercalators. Third, even for the strong binders mentioned earlier, DNA binding affinities could not match that of doxorubicin. Lastly, when the correlation between antiproliferative IC<sub>50</sub> and DC<sub>50</sub> values were examined in a Spearman correlation matrix (Supporting Information Table S3), the magnitude of the ρ values (0.25–0.34) did not point to a convincing relationship between these two activities.

### 3.3. Redox cycling and generation of reactive oxygen species

The quinone moiety is known to accept a single electron to yield the semiquinone radical which can react directly with DNA [37] or participate in a redox cycle of superoxide radical generation by transfer of electrons to oxygen [38]. Superoxide and its dismutation product hydrogen peroxide form hydroxyl radicals, which if generated in the vicinity of DNA can inflict substantial damage [39]. Thus it was of interest to determine if the quinone-bearing dioxonaphthoimidazoliums would predispose the scaffold to free radical generation and redox cycling. Two assay methods were employed – an *in vitro* assay centered on the oxidation of phenol red by hydrogen peroxide [40] and a cell based method for the detection of free radical formation via oxidation of 2', 7' dichlorodihydrofluorescein (H<sub>2</sub>DCF).

In the *in vitro* method, the oxidation of dithiothreitol provides electrons required to reduce the quinone to semiquinone or hydroquinone. This reaction is reversed in the presence of oxygen, generating superoxide anions which dismutate to hydrogen peroxide and oxidize phenol red in the presence of horseradish peroxidase. In the presence of a redox cyler, phenol red is continually oxidized, causing its absorbance at 610 nm to increase. The redox cycling propensity of the test compound was determined by the concentration (EC<sub>50</sub>) required to increase the absorbance of oxidized phenol red at 610 nm to half its maximum value (Table 2). A compound predisposed to facile redox cycling will have a lower EC<sub>50</sub> compared to a weak or non-redox cyler. Representative dose response plots are shown in Supporting Information (Figure S2).

YM155 and its analogs (except for several members in series C) were found to be redox cyclers with EC<sub>50</sub> values in the range of 0.7 μM–13 μM. In this context, YM155 (EC<sub>50</sub> 1.4 μM) was more potent than most of its analogs but compared to a known redox cyler like naphthoquinone (EC<sub>50</sub> 0.33 μM), it was clearly less effective. In terms of the SAR for redox cycling, the series C compounds provided valuable insight. Only two compounds in series C were redox cyclers, namely **C1-1** and **C1-2**. None of the non-quinone bearing series C analogs were redox cyclers but strikingly, some quinone-containing analogs (**C4-1**, **C4-2**) also failed to redox cycle. Since **C4-1** and **C4-2** are not positively charged at N<sup>3</sup>, this would imply that the charged imidazolium and quinone are both necessary for redox cycling. If so, the outstanding activity of naphthoquinone (YM155 without imidazolium) is unexpected. Thus, pending additional data, a reasonable conclusion would be

**Table 2**  
DNA intercalation DC<sub>50</sub> and redox cycling EC<sub>50</sub> values of test compounds.

Compound	DC <sub>50</sub> (μM) <sup>a</sup> for DNA intercalation	EC <sub>50</sub> (μM) <sup>b</sup> for redox cycling
YM155	20.3 ± 3.1	1.38 ± 0.05
<b>A1-1</b>	27.5 ± 0.5	3.63 ± 0.71
<b>A1-2</b>	35.4 ± 1.4	13.0 ± 0.3
<b>A1-3</b>	28.6 ± 0.4	3.22 ± 0.14
<b>A2-1</b>	31.9 ± 1.1	6.27 ± 0.26
<b>A3-1</b>	28.6 ± 3.1	2.10 ± 0.24
<b>A3-2</b>	16.4 ± 1.3	1.91 ± 0.24
<b>A3-3</b>	20.0 ± 0.5	2.01 ± 0.10
<b>A3-4</b>	45.0 ± 3.3	1.36 ± 0.11
<b>A3-5</b>	25.4 ± 2.4	4.56 ± 0.13
<b>A3-6</b>	26.7 ± 3.4	3.09 ± 0.08
<b>A3-7</b>	23.0 ± 1.2	2.37 ± 0.01
<b>A3-8</b>	18.4 ± 1.2	2.57 ± 0.16
<b>A4-1</b>	44.0 ± 3.2	7.58 ± 0.20
<b>A5-1</b>	95.4 ± 7.5	2.96 ± 0.15
<b>A6-1</b>	32.3 ± 3.8	9.30 ± 0.43
<b>A6-2</b>	32.3 ± 1.5	5.70 ± 0.43
<b>A6-3</b>	40.1 ± 4.5	7.08 ± 1.18
<b>A6-4</b>	48.2 ± 6.0	8.47 ± 0.15
<b>A6-5</b>	99.0 ± 0.8	10.2 ± 0.5
<b>A6-6</b>	35.4 ± 4.1	6.37 ± 0.69
<b>A6-7</b>	44.2 ± 0.2	6.37 ± 0.69
<b>A6-8</b>	67.0 ± 5.8	8.75 ± 0.43
<b>B1-1</b>	17.7 ± 1.2	2.36 ± 0.04
<b>B1-2</b>	13.3 ± 0.9	3.67 ± 0.20
<b>B1-3</b>	20.9 ± 1.4	0.68 ± 0.00
<b>B2-1</b>	30.6 ± 0.8	2.94 ± 0.05
<b>B2-2</b>	24.0 ± 2.4	3.32 ± 0.13
<b>B2-3</b>	30.1 ± 1.5	2.26 ± 0.05
<b>B2-4</b>	56.9 ± 9.1	3.47 ± 0.45
<b>B2-5</b>	25.2 ± 1.6	3.92 ± 0.10
<b>B2-6</b>	27.9 ± 3.8	2.31 ± 0.37
<b>B2-7</b>	43.3 ± 2.3	5.82 ± 0.05
<b>B2-8</b>	78.8 ± 13.2	7.35 ± 0.06
<b>B3-1</b>	13.9 ± 0.7	1.85 ± 0.10
<b>B3-2</b>	12.0 ± 1.0	1.34 ± 0.06
<b>B4-1</b>	19.9 ± 4.0	1.43 ± 0.06
<b>B4-2</b>	15.5 ± 0.3	1.01 ± 0.04
<b>C1-1</b>	29.5 ± 2.6	2.00 ± 0.04
<b>C1-2</b>	>100	1.42 ± 0.01
<b>C2-1</b>	>100	>400
<b>C2-2</b>	>100	>400
<b>C2-3</b>	>100	>400
<b>C3-1</b>	>100	>400
<b>C3-2</b>	>100	>400
<b>C4-1</b>	>100	>400
<b>C4-2</b>	>100	>400
<b>AB1</b>	20.8 ± 1.3	6.10 ± 0.38
<b>AB2</b>	21.3 ± 3.2	3.47 ± 0.08
<b>AB3</b>	22.7 ± 1.6	7.61 ± 0.07
<b>AB4</b>	17.6 ± 1.2	3.86 ± 0.11
<b>AB5</b>	14.7 ± 1.5	3.48 ± 0.01
<b>AB6</b>	12.0 ± 0.3	2.75 ± 0.18
<b>AB7</b>	12.7 ± 0.5	7.55 ± 0.71
Doxorubicin	2.64 ± 0.16	Not determined
Naphthoquinone	>100	0.33 ± 0.01

<sup>a</sup> DC<sub>50</sub>: Concentration required to reduce basal fluorescence of thiazole orange (10 μM) by 50%.

<sup>b</sup> EC<sub>50</sub>: Concentration required to reduce oxidized phenol red absorbance to 50% of control values. Mean and SD of n = 3 separate determinations for both experiments. None of the compounds were fluorescent under test conditions.

that the quinone moiety per se is not sufficient to ensure redox cycling.

Another SAR pertains to the requirement of at least one ring-containing substituent at N<sup>1</sup> or N<sup>3</sup> for activity. Analogs with aromatic ring substituents on both imidazole nitrogens (N<sup>1</sup>, N<sup>3</sup>) were generally better redox cyclers (**B3-1**, **B3-2**) than those without this motif (**AB7**, **A6-1** to **A6-8**). Anecdotal comparisons of anti-proliferative IC<sub>50</sub> and redox cycling EC<sub>50</sub> values revealed a disparity between these activities among several analogs. For example **AB1**, **AB2** and **A6-2** which were equipotent to YM155 in terms of antiproliferative activities were less competent redox

cyclers. Conversely, potent redox cyclers like **B1-3** and naphthoquinone had only modest antiproliferative activities. Indeed, when the correlation between these activities was examined in a Spearman correlation matrix (Supporting Information Table S3), the ρ values (−0.002 to −0.129) did not support a meaningful relationship.

Next, we determined if YM155 and selected analogs generated free radicals in a cellular environment. To this end, we pretreated RCC786-0 and H1299 cells with 20 μM 2', 7'-dichlorodihydrofluorescein (H<sub>2</sub>DCF) diacetate and exposed the loaded cells (2 h) to various concentrations of test compounds. Briefly, the diacetate is

hydrolyzed by cellular membrane esterases to give the cell permeant, non-fluorescent H<sub>2</sub>DCF which is oxidized intracellularly by reactive oxygen species (ROS) to the fluorescent product dichlorofluorescein. Hence, an increase in fluorescence would be observed if the test compound generated ROS by redox cycling or other means. Representative compounds (YM155, **A3-3**, **B1-3**, **C1-2**, **AB1**, **AB7**) that have with a range of redox cycling activities were selected for investigation. **B1-3** is a strong redox cyclers (EC<sub>50</sub> 0.68 μM), YM155, **C1-2**, **A3-3** have modest activities (EC<sub>50</sub> 1.4–2 μM) and **AB1**, **AB7** are weaker cyclers (EC<sub>50</sub> 6.1, 7.6 μM). Naphthoquinone was included as positive control. The compounds were tested at concentrations equivalent to 1×, 2×, 5× and 10× antiproliferative IC<sub>50</sub> (Table S1). As seen from Fig. 4, the compounds had strikingly similar effects on both cell lines. In each case, YM155, **A3-3**, **B1-3**, **AB1** and **AB7** did not alter the basal level of fluorescence over the entire concentration range, indicating that under these conditions, these compounds did not generate ROS. In contrast **C1-2** demonstrated a dose dependent increase in

fluorescence matching that of naphthoquinone at 5× IC<sub>50</sub> (RCC786-0) and exceeding it at 2× IC<sub>50</sub> (H1299). We noted that **C1-2**, like naphthoquinone, is a bicyclic quinone and this structural feature which is not found in the other YM155 analogs, could have accounted for its unusual potency. Taken together, both *in vitro* and cell based assays confirmed the significantly weaker redox cycling activities of the dioxonaphthoquinone analogs as compared to naphthoquinone.

#### 3.4. Formation of γH2AX in treated cells

YM155 was reported to intercalate with DNA and to induce a DNA damage response which is purportedly central to its anti-cancer properties [26,28]. In the presence of YM155, prostate cancer cells PC3 showed dose dependent increases in two biomarkers of DNA damage, phosphorylated histone γH2AX and phosphorylated KAP1. These increases were observed at concentrations that did not reduce survivin, thus implicating DNA damage, rather than

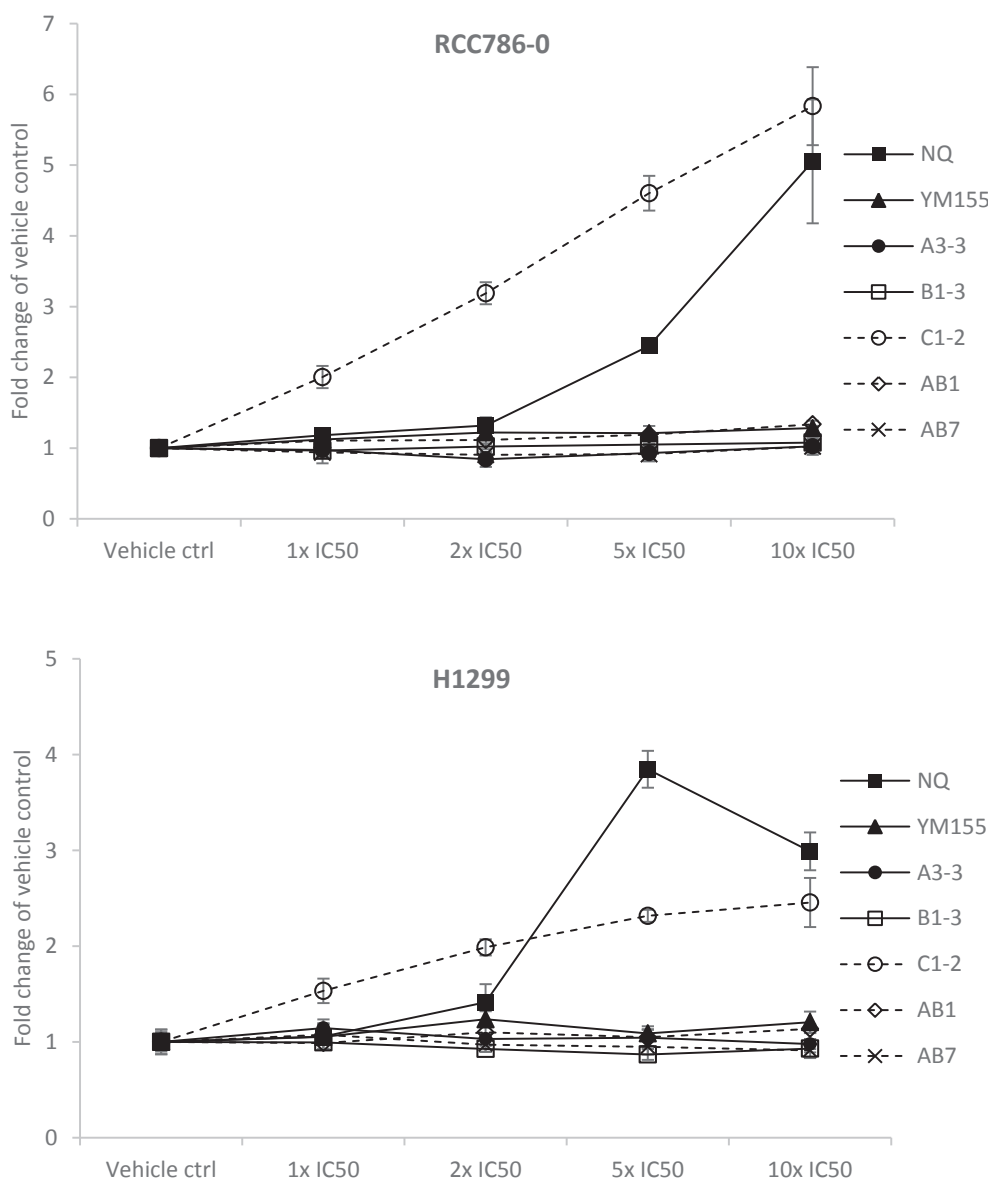


**Fig. 4.** Generation of free radicals in RCC786-0 and H1299 cells at different concentrations of test compounds as determined by the fold change in H<sub>2</sub>DCF fluorescence. The fold change of fluorescence over vehicle control at each concentration is displayed as the mean with SD of n = 3 determinations.

suppression of survivin, as the initiating event. We have shown that YM155 and several analogs had the capacity to intercalate with DNA but with weaker affinities compared to doxorubicin. To determine if intercalation is followed by DNA damage, we monitored levels of  $\gamma$ H2AX (a marker for double strand breaks in DNA) [41,42] in RCC786-0 and H1299 cells treated with YM155, **AB1** and **AB7**. In terms of  $IC_{50}$ , **AB1** was more potent than YM155 (36 nM versus 54 nM) but comparable to it on H1299 (36 nM for both). **AB7** was more potent than YM155 on both cell lines.  $\gamma$ H2AX levels also increase in response to DNA fragmentation which is a sequel of apoptosis [43,44]. As such it is necessary to establish if the elevated  $\gamma$ H2AX levels in treated cells is a consequence of DNA damage or DNA fragmentation due to apoptosis. In general, DNA damage is initiated more rapidly than apoptotic cell death. Thus, time-based experiments in which levels of an apoptotic marker cleaved caspase 3 and  $\gamma$ H2AX from treated cells were concurrently monitored.

Fig. 5 shows the levels of  $\gamma$ H2AX, cleaved caspase 3 and survivin in RCC786-0 (panels A, B) and H1299 cells (panels C, D) treated for various time periods with YM155, **AB1** and **AB7** at their  $IC_{50}$  concentrations. The appearance of  $\gamma$ H2AX was time dependent on both cell lines. In RCC786-0,  $\gamma$ H2AX was detected at 24 h but only in YM155-treated cells. In the case of **AB1** and **AB7**,  $\gamma$ H2AX appeared later at 48 h. Cleaved caspase 3 levels in treated RCC786-0 cells were found to increase in tandem with  $\gamma$ H2AX. In H1299 cells,  $\gamma$ H2AX was detected at only 48 h (**AB1** and **AB7**) and 72 h (YM155). We noted again that increases in cleaved caspase 3 and  $\gamma$ H2AX were synchronized. Survivin levels were also tracked and found to decrease before  $\gamma$ H2AX was detected (RCC786-0) or at the same time (H1299).

Next we investigated the effects of varying the concentrations ( $0.5\times$ ,  $1\times$ ,  $2\times$   $IC_{50}$ ) of YM155 and **AB1** on the expression of  $\gamma$ H2AX in the same cell lines at a fixed time of 48 h. Dose dependent increases in  $\gamma$ H2AX were observed for both compounds (Supporting Information, Figure S3). These increases were aligned to increases in cleaved caspase 3 and decreases in survivin levels. Thus, YM155, **AB1** and **AB7** induced time-dependent increases in  $\gamma$ H2AX levels in both RCC786-0 and H1299 cells. Increases coincided with the elevation in levels of cleaved caspase 3 and were

observed at the same time or after declines in survivin. In YM155 and **AB1**-treated cells, increases in  $\gamma$ H2AX were also concentration dependent.

### 3.5. YM155 and selected analogs induced apoptosis in RCC786-0 cells

A multiplex assay (ApoTox-Glo™) was used to simultaneously monitor cell viability, cytotoxicity and apoptotic events in RCC786-0 cells that were exposed (48 h) to varying concentrations of YM155, **A4-1**, **B2-4** and **AB1** (Supporting Information, Figure S4). The test compounds displayed similar trends in their concentration dependent effects on viability, cytotoxicity and apoptosis. Cell viability decreased with increasing concentrations while cytotoxicity remained at basal levels except at the highest concentrations of YM155 and **AB1**. Apoptotic events were monitored by the activation of caspases 3 and 7 and here, activation was observed to increase in tandem with the decline in cell viability. These results showed that loss in cell viability was largely due to apoptosis with negligible contribution from necrotic cell death.

### 3.6. Transcriptome analysis of YM155-treated RCC786-0 cells

To further determine if the DNA damage response was critical to the mode of action of YM155, we compared the transcriptional profile of RCC786-0 cells that were treated with YM155 at its  $IC_{50}$  (40 nM) for 24 h with control untreated cells. Genes that were significantly altered in the treated cells by 2-fold or more (adjusted p-value < 0.05) were identified and subjected to pathway analysis. Several canonical signaling pathways were significantly affected by YM155, including the p53 and ErbB signaling pathways (Supporting Information, Figure S5). We further mined the data for genes that were involved in DNA repair. Of the 257 DNA repair genes that were curated, we found significant up-regulation of HES1 (2.24-fold) and PER (2.15-fold). Notably, these two genes were not involved in the repair of double-stranded breaks. Genes involved in double-stranded break repair, such as MRE11 (-1.64-fold) and RAD50 (1.26-fold) were minimally up- or down-regulated. Indeed, an

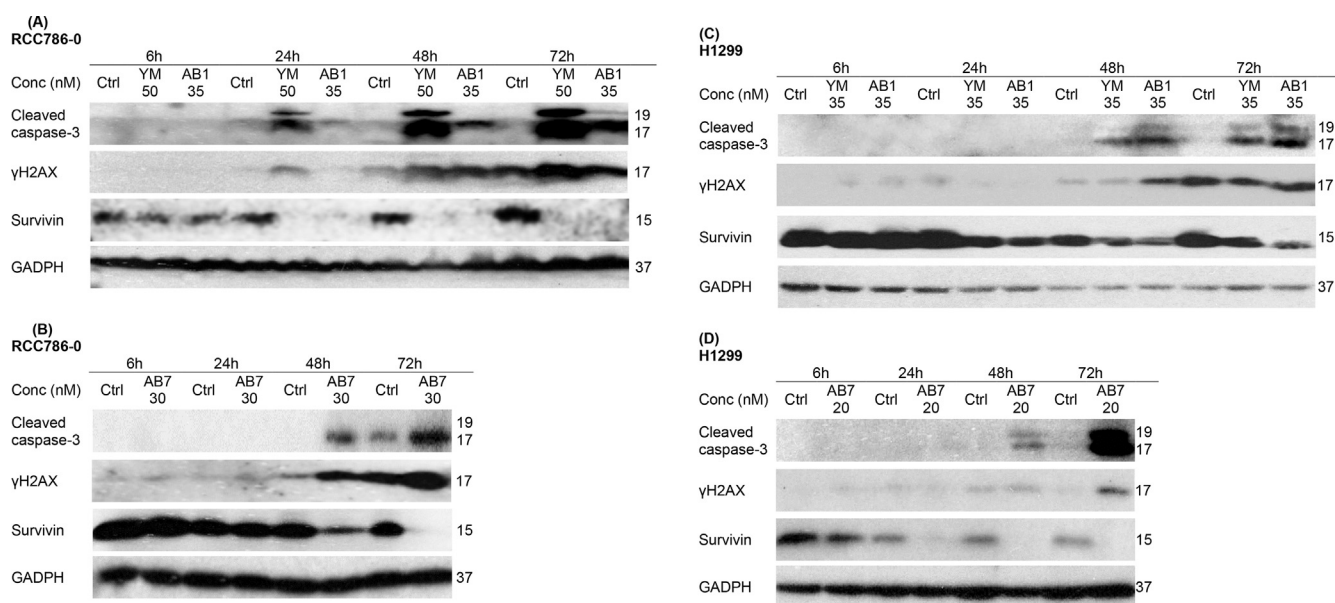


Fig. 5. YM155, **AB1** and **AB7** induced time dependent increases in  $\gamma$ H2AX in RCC786-0 (panels A, B) and H1299 cells (panels C, D). Cells were incubated with test compounds at their  $IC_{50}$  concentrations for 6, 24, 48 and 72 h, after which  $\gamma$ H2AX, survivin and cleaved caspase 3 levels (p17, p19) were probed by immunoblotting. The p19 fragment is the precursor of p17. GADPH was used as loading control. Molecular weights are shown on the right hand side of the blots.

overwhelming majority of the genes involved in DNA repair were not strongly perturbed by YM155 treatment (Supporting Information, Table S4).

#### 4. Discussion

YM155 was identified as a specific repressor of survivin promoter activity in an artificial reporter system containing the survivin promoter [45]. Ensuing investigations showed that tumor regressions induced by YM155 in xenograft models were associated with diminished intratumoral survivin expression levels [46]. Despite its outstanding potency in preclinical studies, YM155 performed disappointingly in clinical trials [21]. Recent findings have shown that the uptake of YM155 into cells was dependent on the presence of a specific solute carrier SLC35F2 and it is conceivable that varying levels of this transporter on the outer membrane surfaces of tumoral cells could have moderated the cytotoxicity of YM155 [28]. Various reports have since questioned if the suppression of survivin is the sole and main effect of YM155-induced cytotoxicity [21,26,28]. The consensus is that YM155 is a DNA intercalating agent and induces a DNA damage response that leads to apoptotic cell death. In this report, we adopted an SAR approach to assess the contribution of DNA intercalation and redox cycling which are incipient events in the DNA damage response, to the antiproliferative activities of YM155 and its analogs. The premise was that overlapping structural requirements would support a prominent role for DNA damage in the antiproliferative activity of YM155.

The structural requirements for growth inhibition were deduced from the activities of YM155 and its analogs on four malignant cell lines that belonged to two cancer types. A common finding was that the intact dioxonaphthoimidazolium scaffold was required for activity. Of the various motifs on the tricyclic scaffold, the quinone was recognized as the most critical, followed by the positively charged imidazolium and lastly, the benzene ring. Greater diversity was tolerated at the N<sup>1</sup> and N<sup>3</sup> side chains of the scaffold. A striking SAR trend that applied to both positions was the marked preference for short, unbranched and cyclized alkyl groups. In fact, this was the only acceptable modification of the 2'-methoxyethyl side chain at N<sup>1</sup>. Greater leeway was permitted at the N<sup>3</sup> position which accepts short unbranched alkyl groups as well as isosteric modifications of the pyrazine-2'-ylmethyl side chain.

Analysis of the SAR for intercalation and growth inhibition revealed that aside from a common requirement for an intact scaffold, there were few overlapping structural features for these two activities. A case in point is the marked preference for cyclized or bulky substituents at N<sup>1</sup>, C<sup>2</sup> and N<sup>3</sup> which was not favored for growth inhibition. It is noted however that minimally substituted **AB7** was an exception and demonstrated strong intercalation and growth inhibition. Limited overlaps were observed in the SAR for redox cycling and growth inhibition. Notably, there is less certainty as to whether the intact scaffold is required for redox cycling or even if the presence of quinone will ensure redox cycling. Furthermore, ring bearing groups on N<sup>1</sup> and N<sup>3</sup> were yet again preferred for redox cycling whereas these same groups adversely affected growth inhibition. Taken together, the present results do not convincingly point to overlapping structural requirements for growth inhibition and DNA intercalation or redox cycling. YM155 and its potent dioxonaphthoimidazolium analogs (**A3-3**, **AB1**, **AB7**) are modest DNA intercalators with limited capacities to generate free radicals. The latter was confirmed in cell based assays, lending further support to the notion that free radical generation does not contribute significantly to the cellular effects of these compounds.

Notwithstanding these SAR deductions, YM155, **AB1** and **AB7** elevated levels of the DNA damage marker  $\gamma$ H2AX in treated cells.

However, these increases were not entirely compatible with the DNA damage response for several reasons. First, they were delayed in terms of detection in treated cells and second, they were closely aligned to the appearance of the apoptotic marker protein cleaved caspase 3. This raises the possibility that the elevation of  $\gamma$ H2AX is due to DNA fragmentation which is a sequel of apoptotic cell death [43,47–49]. Further insight was gained from the transcriptional profile of RCC786-0 cells treated with YM155. Analysis of the DNA repair genes revealed significant up-regulation of only a limited number of genes involved in DNA repair (HES1, PER) while the majority were either down-regulated or unaltered. Hence, DNA damage is not as pervasive as anticipated. We noted that others have also found DNA damage in only a fraction of cells treated with YM155 in comet assays [28]. As anticipated, downregulation of survivin was observed in cells treated with YM155, **AB1** and **AB7**. The decreases in survivin were closely aligned to the appearance of cleaved caspase 3 and either preceded the appearance of  $\gamma$ H2AX or were observed concurrently. That the minimally substituted **AB7** evoked down-regulation of survivin and many other properties associated with YM155 pointed to the sufficiency of the pared down dioxonaphthoimidazolium scaffold for activity.

In conclusion, we have shown that YM155 and its dioxonaphthoimidazolium analogs are modest DNA intercalators with limited potential as redox cyclers. Intercalation per se does not directly result in DNA damage but it does promote unwinding of the DNA helix which would render it susceptible to events (misreading, mutations, interference with transcription and replication) that perturb the transcription of gene products in canonical pathways that are essential for cell survival. Thus, the capacity of functionalized dioxonaphthoimidazoliums to inflict direct DNA damage leading to cell death should be reconsidered. While it would be remiss to disregard DNA as a target of YM155 and its dioxonaphthoimidazolium analogs, its role in the antiproliferative activities of these compounds may not be as significant as originally proposed. Neither do our results refute the survivin suppressant properties of YM155 and its analogs. Rather, they point to the possibility that survivin is not the only gene product whose transcription is disrupted by these compounds.

#### 5. Experimental section

##### 5.1. General details for chemical synthesis

Reagents (synthetic grade or better) were obtained from commercial sources and used without further purification. Reactions were monitored by thin layer chromatography using pre-coated aluminum plates (silica gel 60, F254, Merck). Column chromatography on silica gel 60 (230–400 mesh, Merck) was used for compound purification. <sup>1</sup>H NMR spectra (400 MHz) and <sup>13</sup>C spectra (100 MHz) were recorded on a Bruker Avance 400 Ultrashield instrument (Bruker, Billerica, MA, USA), and referenced to residual solvent peaks. Nominal mass information was captured on an AB Sciex QTrap 2000 mass spectrometer (AB Sciex, Framingham, MA, USA) by electrospray ionization (ESI). Accurate mass information was captured on a Bruker micrOTOFQII mass spectrometer (Bruker, Billerica, MA, USA) by ESI. Compound purity was ascertained on a reverse-phase HPLC on a Shimadzu Nexera SR HPLC system (Shimadzu Scientific Instruments, Columbia, MD, USA) with a Zorbax Eclipse XDB-C18 column (Agilent Tech. Inc., Loveland, CO) at two wavelengths: 254 and 280 nm. Each test compound was evaluated on two of four isocratic solvent systems: System A: 60% MeOH + 40% water, with 15 mM ammonium formate; System B: 30% MeOH + 30% CH<sub>3</sub>CN + 40% water, with 15 mM ammonium formate; System C: 60% MeOH + 40% water; System D: 60% CH<sub>3</sub>CN + 40% water. Compounds with peak areas  $\geq$ 95% on two

solvent systems were deemed sufficiently pure for biological investigations. The purity of **C2-3** was determined by elemental analysis (C, H, N) on the Elementar Vario Micro Cube instrument (Elementar Analysensysteme GmbH, Hanau, Germany) and found to be within  $\pm 0.4\%$  of expected values. Spectral and nominal mass data are provided in the [Supporting Information](#).

#### 5.1.1. 2-Chloro-3-(methylamino)-1,4-naphthoquinone (**7**)

To 2,3-dichloro-1,4-naphthoquinone (0.341 g, 1.50 mmol) in 1.5 ml of ethanol was added methylamine (0.0465 g, 1.50 mmol) and triethylamine (0.227 g, 2.25 mmol) and the mixture stirred at r.t. for 18 h. The red precipitate formed was filtered under suction, washed with distilled water and dried to afford (**7**) as a red solid, 91.0%.  $^1\text{H}$  (CDCl<sub>3</sub>)  $\delta$  8.15 (dd, 1H,  $J = 0.90, 7.69$  Hz), 8.03 (dd, 1H,  $J = 0.94, 7.67$  Hz), 7.72 (dt, 1H,  $J = 1.34, 7.60$  Hz), 7.62 (dt, 1H,  $J = 1.31, 7.56$  Hz), 6.10 (br s, 1H), 3.45 (d, 3H,  $J = 5.60$  Hz);  $^{13}\text{C}$  (CDCl<sub>3</sub>)  $\delta$  180.53, 144.89, 134.94, 132.78, 132.45, 132.39, 129.74, 126.84, 126.76, 32.55.

#### 5.1.2. 2-Chloro-3-cyclopropylamino-1,4-naphthoquinone (**11**)

To 2,3-dichloro-1,4-naphthoquinone (0.341 g, 1.50 mmol) in 1.5 ml of ethanol was added cyclopropylamine (0.0856 g, 1.50 mmol) and triethylamine (0.227 g, 2.25 mmol) and the mixture stirred at r.t. for 18 h. The red precipitate formed was filtered under suction, washed with distilled water and dried to afford (**11**) as a red solid, 93.9%.  $^1\text{H}$  (CDCl<sub>3</sub>)  $\delta$  8.16 (dd, 1H,  $J = 1.11, 7.69$  Hz), 8.02 (dd, 1H,  $J = 1.23, 7.67$  Hz), 7.72 (dt, 1H,  $J = 1.31, 7.61$  Hz), 7.62 (dt, 1H,  $J = 1.28, 7.57$  Hz), 6.12 (br s, 1H), 3.34–3.28 (m, 1H), 0.97–0.92 (m, 2H), 0.78–0.73 (m, 2H);  $^{13}\text{C}$  (CDCl<sub>3</sub>)  $\delta$  180.27, 177.14, 145.07, 134.91, 132.74, 132.46, 129.75, 126.92, 126.72, 111.52, 27.43, 10.40.

#### 5.1.3. N-(3-chloro-1,4-dioxo-1,4-dihydro-naphthalen-2-yl)-N-methyl-acetamide (**19**)

Two drops of concentrated sulfuric acid were added to a suspension of (**7**) (0.443 g, 2.00 mmol) in acetic anhydride (1.84 g, 18.0 mmol) and stirred for 1.5 h at r.t. 10 ml of distilled water was added slowly to the reaction mixture with stirring to quench excess anhydride, and extracted with EtOAc. The organic layer was washed with saturated NaHCO<sub>3</sub> solution and brine and dried over anhydrous Na<sub>2</sub>SO<sub>4</sub>. Purification by column (1:4 EtOAc/Hexanes) afforded (**19**) as a yellow solid, 92.6%.  $^1\text{H}$  (CDCl<sub>3</sub>)  $\delta$  8.28–8.08 (m, 2H), 7.86–7.77 (m, 2H), 3.19 (s, 3H), 1.93 (s, 3H);  $^{13}\text{C}$  (CDCl<sub>3</sub>)  $\delta$  183.10, 179.16, 177.84, 134.89, 134.77, 134.72, 134.69, 134.62, 134.16, 131.31, 127.57, 40.11, 21.76.

#### 5.1.4. N-(3-chloro-1,4-dioxo-1,4-dihydro-naphthalen-2-yl)-N-cyclopropyl-acetamide (**23**)

Two drops of concentrated sulfuric acid were added to a suspension of (**11**) (0.495 g, 2.0 mmol) in acetic anhydride (1.84 g, 18.0 mmol) and stirred for 1.5 h at r.t. 10 ml of distilled water was added slowly to the reaction mixture with stirring to quench excess anhydride, and extracted with EtOAc. The organic layer was washed with saturated NaHCO<sub>3</sub> solution and brine and dried over anhydrous Na<sub>2</sub>SO<sub>4</sub>. Purification by column (1:4 EtOAc/Hexanes) afforded (**23**) as yellow plates, 89.1%.  $^1\text{H}$  (CDCl<sub>3</sub>)  $\delta$  8.20–8.12 (m, 2H), 7.84–7.74 (m, 2H), 3.27–3.17 (m, 1H), 2.43 (s, 3H), 0.98–0.68 (m, 4H);  $^{13}\text{C}$  (CDCl<sub>3</sub>)  $\delta$  178.01, 134.81, 134.66, 134.56, 134.46, 134.29, 131.40, 131.15, 127.43, 127.40, 31.31, 22.33, 8.86, 8.60.

#### 5.1.5. N-cyclopropyl-N-[1,4-dioxo-3-[(pyridin-4-ylmethyl)-amino]-1,4-dihydro-naphthalen-2-yl]-acetamide (**64**)

To a suspension of (**23**) (0.955 g, 3.30 mmol) in 5 ml of toluene was added pyridin-4-ylmethylamine (0.535 g, 4.95 mmol) and triethylamine (0.500 mg, 4.95 mmol) and stirred at 45 °C for 2 h. The reaction mixture was cooled, and the precipitate was filtered

under suction and washed with EtOH and distilled water to afford (**64**) as a yellow-brown solid, which was unstable and used immediately for the next step.

#### 5.1.6. N-[1,4-dioxo-3-methylamino-1,4-dihydro-naphthalen-2-yl]-N-methyl-acetamide (**70**)

To a stirred suspension of (**19**) (0.400 g, 1.52 mmol) in 2 mL of toluene was added dropwise methylamine (0.0564 g, 1.82 mmol) and triethylamine (0.230 g, 2.28 mmol). The mixture was stirred at r.t. for 1 h. The precipitate was filtered under suction, washed with distilled water and EtOH to afford (**70**) as red solids, 62.0%.  $^1\text{H}$  (CDCl<sub>3</sub>)  $\delta$  8.15 (dd, 1H,  $J = 0.83, 7.70$  Hz), 8.08 (dd, 1H,  $J = 0.87, 7.70$  Hz), 7.78 (dt, 1H,  $J = 1.33, 7.59$  Hz), 7.66 (dt, 1H,  $J = 1.30, 7.56$  Hz), 6.24 (br s, 1H), 3.13 (s, 3H), 3.11 (d, 3H,  $J = 5.78$  Hz), 1.99 (s, 3H);  $^{13}\text{C}$  (CDCl<sub>3</sub>)  $\delta$  182.30, 179.35, 172.36, 144.11, 135.47, 132.77, 132.66, 130.14, 126.86, 126.76, 118.44, 37.50, 30.65, 21.94.

#### 5.1.7. 1-Cyclopropyl-2-methyl-4,9-dioxo-3-(pyridin-4-ylmethyl)-4,9-dihydro-1H-naphtho[2,3-d]imidazol-3-ium hydrogen dibromide (**AB1**)

48% Hydrobromic acid (30.0 mmol) was added dropwise to a solution of crude (**64**) in a 4 mL mixture of 1:1 EtOH/EtOAc and stirred at 45 °C for 4 h and subsequently r.t. for an additional 12 h. The reaction mixture was concentrated *in vacuo* and purified by column chromatography (8:92 MeOH/CH<sub>2</sub>Cl<sub>2</sub>) to afford (**AB1**) as a yellow solid, 22.0%.  $^1\text{H}$  (D<sub>6</sub>-DMSO)  $\delta$  8.76 (d, 2H,  $J = 6.36$  Hz), 8.23 (dd, 1H,  $J = 1.14, 7.65$  Hz), 8.09 (dd, 1H,  $J = 1.33, 7.49$  Hz), 8.01 (dt, 1H,  $J = 1.55, 7.55$  Hz), 7.96 (dt, 1H,  $J = 1.44, 7.47$  Hz), 7.72 (d, 2H,  $J = 6.35$  Hz), 6.08 (s, 2H), 3.77–3.71 (m, 1H), 2.90 (s, 3H), 1.43–1.38 (m, 2H), 1.30–1.26 (m, 2H);  $^{13}\text{C}$  (D<sub>6</sub>-DMSO)  $\delta$  174.87, 173.50, 155.98, 147.98, 146.17, 135.58, 135.11, 132.51, 132.09, 131.24, 129.62, 127.16, 126.76, 123.23, 49.16, 29.84, 11.85, 9.00. ESI-MS:  $m/z$  344.1 [M–Br]<sup>+</sup>. High resolution MS (ESI) calcd for C<sub>21</sub>H<sub>18</sub> BrN<sub>3</sub>O<sub>2</sub> [M–Br]<sup>+</sup> 344.1394. Found: 344.1405. HPLC purity: system A: 99.85% (254 nm), 100.00% (280 nm); system B: 99.38% (254 nm), 99.40% (280 nm).

#### 5.1.8. 1,2,3-Trimethyl-4,9-dioxo-4,9-dihydro-1H-naphtho[2,3-d]imidazol-3-ium bromide (**AB7**)

48% hydrobromic acid (10.0 mmol) was added dropwise to a solution of (**70**) (0.263 mg, 1.0 mmol) in a 1.5 ml mixture of 1:1 EtOH/EtOAc and stirred at 40 °C for 4 h followed by r.t. for an additional 12 h. The reaction mixture was concentrated *in vacuo* and purified by column chromatography (8:92 MeOH/CH<sub>2</sub>Cl<sub>2</sub>) to afford (**AB7**) as a beige solid, 21.9%.  $^1\text{H}$  (D<sub>6</sub>-DMSO)  $\delta$  8.18 (dd, 1H,  $J = 3.31, 5.73$  Hz), 7.99 (dd, 1H,  $J = 3.31, 5.74$  Hz), 4.13 (s, 6H), 2.79 (s, 3H);  $^{13}\text{C}$  (D<sub>6</sub>-DMSO)  $\delta$  175.36, 153.39, 135.60, 131.91, 130.34, 127.18, 34.37, 10.17. High resolution MS (ESI) calcd for C<sub>14</sub>H<sub>13</sub> BrN<sub>2</sub>O<sub>2</sub> [M–Br]<sup>+</sup> 241.0972. Found 241.0967. HPLC purity: system A: 99.83% (254 nm), 99.89% (280 nm); system B: 99.74% (254 nm), 99.74% (280 nm).

## 5.2. Biological assays

### 5.2.1. General biology

Dulbecco's Modified Eagle's Media (DMEM) and Roswell Park Memorial Institute Media 1640 (RPMI-1640) were purchased from Caisson Laboratories Inc. (North Logan, UT) and supplemented with 10% heat inactivated fetal bovine serum (FBS) (Gibco, Life Technologies Corporation, Carlsbad, CA, USA) and 0.01% w/v Penicillin-G-Streptomycin mixture (GE Healthcare, Buckinghamshire, United Kingdom). 3-(4,5-Dimethylthiazol-2-yl)-2,5-diphenyltetrazolium bromide (MTT) was purchased from Alfa Aesar, Inc. (Lancashire, United Kingdom), reconstituted in phosphate-buffered saline to 2 mg/mL and diluted with appropriate cell culture media before

use. Herring sperm DNA and the Apotax-Glo™ assay kit were obtained from Promega Ptd. Ltd. (Madison, WI, USA). Doxorubicin, naphthoquinone, thiazole orange, phenol red sodium, dithiothreitol and horseradish peroxidase (HRP) were purchased from Sigma–Aldrich (St. Louis, MO, USA). 2', 7'-Dichlorodihydrofluorescein diacetate (H<sub>2</sub>DCF DA) was purchased from Life Technologies Corporation (Carlsbad, CA, USA). Anti-cleaved caspase-3 and anti-γH2AX antibodies were obtained from Cell Signalling Technology Inc. (Danvers, MA, USA) and anti-GADPH antibody was from Santa Cruz Biotechnology Inc. (Santa Cruz, CA, USA).

### 5.2.2. Cell culture

Human clear cell renal cell carcinoma cell lines RCC786-0, RCC4/VA, non-small cell lung carcinoma cell lines H1299, H1666 and proliferating normal lung fibroblasts IMR-90 cells were obtained from American Type Culture Collection (ATCC, Rockville, MD). RCC786-0, RCC4/VA and IMR-90 cells were cultured in complete DMEM. H1299 and H1666 cells were cultured in complete RPMI-1640 and incubated at 37 °C, 5% CO<sub>2</sub>. Malignant and IMR-90 cell lines were sub-cultured at ratios of 1:6 and 1:3 respectively on reaching 90% confluence.

### 5.2.3. MTT assay

Cells were seeded at a density of  $3.0 \times 10^3$  cells/well for malignant cell lines and  $4.0 \times 10^3$  cells/well for IMR-90 in 96-well plates containing 100 μL media per well and incubated for 24 h (37 °C, 5% CO<sub>2</sub>) for cell adherence. After 24 h, media in each well was removed by aspiration and 199 μL of fresh media was added. 1 μL of test compound (prepared in DMSO stock solutions at 200-fold higher concentrations) was added to each well. The final DMSO concentration in each well was kept at 0.5% v/v. The compound-treated cells were incubated for 72 h (37 °C, 5% CO<sub>2</sub>), media was subsequently removed by aspiration and an aliquot (200 μL) of 0.5 mg/mL MTT in media was added to each well. The treated plates were incubated for 2 h (malignant cells) or 3 h (IMR-90 cells) after which the MTT containing media was removed by aspiration and 100 μL of DMSO added to each well to dissolve the purple formazan crystals. Plates were agitated at 700 rpm, 5 min on a plate shaker before absorbance readings were read (570 nm, Tecan Infinite™ M200 Pro). Viable cells were determined from the following equation:

$$\text{Percentage viability} = \left[ \frac{(\text{Ab}_{\text{compound}} - \text{Ab}_{\text{blank}})}{(\text{Ab}_{\text{control}} - \text{Ab}_{\text{blank}})} \right] \times 100\%$$

where  $\text{Ab}_{\text{compound}}$  = Absorbance of compound-treated cells,  $\text{Ab}_{\text{control}}$  = Absorbance of untreated/control cells and  $\text{Ab}_{\text{blank}}$  = Absorbance of DMSO.

Each test compound was assessed at 8 concentrations in at least 3 separate experiments carried out at different times. Cells were from different passage numbers and each compound was tested from 2 stock solutions. For each experiment, percentage viability was calculated using the mean absorbance value from three technical repeats at a given test concentration. The IC<sub>50</sub> (the concentration of test compound required to inhibit cell growth by 50%) was determined by plotting % viability against logarithmic concentration of test compound (GraphPad Prism 5, San Diego, CA).

### 5.2.4. Fluorescent intercalator displacement assay to assess binding to DNA

Previously reported methods were followed with modifications [37,38]. To each well in a black 96-well plate was added 98.5 μL of BPE buffer (comprising 6.0 mM Na<sub>2</sub>HPO<sub>4</sub>, 2.0 mM NaH<sub>2</sub>PO<sub>4</sub>, 1.0 mM

Na<sub>2</sub>EDTA; total Na<sup>+</sup> concentration 16.0 mM; pH 7.0) containing 2 mg/mL herring sperm DNA and 1 μL of 10 μM thiazole orange (ThO) in deionized water. The resulting mixture was incubated at room temperature (25°) for 5 min. 0.5 μL of compound (200-fold concentration in DMSO) was added, kept at room temperature for 8 min, with agitation (500 rpm on a plate shaker) and fluorescence read at  $\lambda_{\text{excitation}} = 503$  nm,  $\lambda_{\text{emission}} = 536$  nm on a microplate reader (Tecan Infinite™ M200 Pro). DMSO per well was kept at 0.5% v/v. Test compound and doxorubicin (positive control) were tested over a range of concentrations in at least 3 separate experiments. The percentage of undisplaced thiazole orange at a specific concentration of test compound was determined from the expression:

$$\% \text{Undisplaced thiazole orange} = \text{RFU}_{\text{compound}} / \text{RFU}_{\text{control}} \times 100\%$$

where  $\text{RFU}_{\text{compound}}$  = fluorescence of test compound and thiazole orange, and  $\text{RFU}_{\text{control}}$  = fluorescence of thiazole orange without test compound. The DC<sub>50</sub> of test compound (concentration required to reduce basal fluorescence of thiazole orange (10 μM) by 50%) was determined by plotting % undisplaced thiazole orange against logarithmic concentration of test compound. (GraphPad Prism 5, San Diego, CA).

### 5.2.5. Horseradish peroxidase-phenol red redox cycling assay

The method described by Johnston et al. [40] and Soares et al. [50] were followed with modifications. 2 μL test compound (200-fold concentration in DMSO), 18 μL Hank's Balanced Salt Solution (HBSS) and 40 μL dithiothreitol (DTT) solution (2.5 mM in HBSS) were sequentially added to each well in a 96-well clear plate. The contents were shaken for 45 min at 600 rpm on a plate shaker, after which was immediately added 40 μL of horseradish peroxidase-phenol red solution (150 μg/mL horseradish peroxidase, 1 mM phenol red sodium in HBSS) and the plate shaken again for another 10 min at 600 rpm. 15 μL 1 M NaOH was added to each well, agitated (1 min) and absorbance readings were read at 610 nm on a microplate reader (Tecan Infinite™ M200 Pro). DMSO content per well was kept at 1% v/v. Test compound and positive control naphthoquinone were tested over a range of concentrations, with at least three separate experiments performed for each concentration. The absorbance at 610 nm was plotted against logarithmic concentration of test compound (GraphPad Prism 5, San Diego, CA) from which EC<sub>50</sub> (concentration required to reduce oxidized phenol red absorbance to 50% of control value) was determined.

### 5.2.6. H<sub>2</sub>DCF-DA assay

RCC786-0 and H1299 cells were seeded at  $1.0 \times 10^4$  cells/well and  $1.5 \times 10^4$  cells/well respectively in black-walled, clear-bottom 96-well cell culture plates and incubated for 24 h at 37 °C, 5% CO<sub>2</sub> in 100 μL of media. 2 μL H<sub>2</sub>DCF-DA in DMSO was then added to each well to give a final concentration of 20 μM and cells were incubated for another hour. The media was removed by aspiration and replaced by 100 μL of pre-warmed PBS containing test compound and 0.5% v/v of DMSO. After incubation for 2 h, plates were read using a microplate reader (Tecan Infinite™ M200 Pro) at  $\lambda_{\text{excitation}} = 495$  nm,  $\lambda_{\text{emission}} = 526$  nm. Test compounds were tested at concentrations corresponding to 1×, 2×, 5× and 10× cell-based IC<sub>50</sub> and fluorescence at each concentration was expressed as fold-change of control fluorescence recorded in untreated cells. Each concentration was investigated in three separate experiments.

### 5.2.7. Western blotting

RCC786-0 and H1299 cells were seeded at a cell density of  $5.0 \times 10^5$  cells/plate in 100 mm petri dishes (24 h, 37 °C, 5% CO<sub>2</sub>) containing 5 mL of media. The media was removed by aspiration

and replaced by 10 mL of fresh media containing test compound and 0.5% v/v of DMSO. After incubation for the indicated times (6, 24, 48 or 72 h), cells were harvested and lysed in Cellytic M<sup>®</sup> buffer (Sigma–Aldrich, St. Louis, MO, USA). Protein content was assessed by Bradford assay and subjected to SDS-PAGE. Cells were blocked in 5% non-fat milk and probed with anti-cleaved caspase-3 or anti- $\gamma$ H2AX antibodies (1:1000 dilution) to determine protein levels. Anti-GADPH antibody was used as a loading control.

### 5.2.8. Transcriptome analysis

Total RNA was isolated using the RNeasy Plus Mini kit (Qiagen GmbH, Hilden, Germany). mRNA was quantified using BioSPEC-Mini (Shimadzu) and its quality evaluated using the Agilent 2100 Bioanalyzer (Agilent Technologies). The samples were processed using Affymetrix 3' IVT Express to create biotin-labeled amplified RNA, which was subsequently fragmented and hybridized to Affymetrix PrimeView Human Gene Expression Arrays (16 h, 45 °C, 60 rpm). Arrays were scanned using an Affymetrix 3000 7G scanner. Data processing was conducted on the Partek Genomics Suite V6.3 (Partek, St Louis, MI). The raw expression values obtained were processed using the Robust Multi-chip Average (RMA) method [51]. p Values for individual genes were adjusted using the Benjamini and Hochberg method. A list of significantly perturbed genes ( $p < 0.05$  and fold change  $> 2$ ) was generated and pathway analysis conducted using the Ingenuity Pathway Analysis (IPA) knowledge base. The significance of the association between the input data set and the functions or pathways was determined by two parameters: (i) the ratio of the number of genes from the data set that map to the function/pathway divided by the total number of genes that map to the function/pathway and (ii) p-value calculated using Fisher's exact test to determine the probability that the association between the genes in the data set and the function/pathway arose by chance alone.

### Acknowledgments

The authors gratefully acknowledged funding support from National University of Singapore (ML Go, R148000188112) and SingHealth Foundation (SPJ Yuen, SHF/FG462P/2011), and Ministry of Education for provision of the National University of Singapore President Graduate Fellowship to Sherman Ho.

### Appendix A. Supplementary data

Supplementary data related to this article can be found at <http://dx.doi.org/10.1016/j.ejmech.2015.09.026>.

### References

- [1] C.H.A. Cheung, L.T. Cheng, K.Y. Chang, H.H. Chen, J.Y. Chang, Investigations of survivin: the past, present and future, *Front. Biosci.* 16 (2011) 952–961.
- [2] J.M. Hernandez, J.M. Farma, D. Coppola, A. Hakam, W.J. Fulp, D.T. Chen, E.M. Siegel, T.J. Yeatman, D. Shibata, Expression of the antiapoptotic protein survivin in colon cancer, *Clin. Colorectal Cancer* 10 (2011) 188–193.
- [3] B.M. Ryan, N. O'Donovan, M.J. Suffy, Survivin: a new target for anti-cancer therapy, *Cancer Treat. Rev.* 35 (2009) 553–562.
- [4] A.C. Mita, M.M. Mita, S.T. Nawrocki, F.J. Giles, Survivin: key regulator of mitosis and apoptosis and novel target for cancer therapeutics, *Clin. Cancer Res.* 14 (2008) 5000–5005.
- [5] S. Weikert, M. Schrader, H. Krause, W. Schulze, M. Muller, K. Miller, The inhibitor of apoptosis (IAP) survivin is expressed in human testicular germ cell tumors and normal testes, *Cancer Lett.* 223 (2004) 331–337.
- [6] S.P. Tu, X.H. Jiang, M.C.M. Lin, J.T. Cui, Y. Yang, C.T. Lum, B. Zou, Y.B. Zhu, S.H. Jiang, W.M. Wong, A.O.O. Chan, M.F. Yuen, S.K. Lam, H.F. Kung, B.C.Y. Wong, Suppression of survivin expression inhibits *in vivo* tumorigenicity and angiogenesis in gastric cancer, *Cancer Res.* 63 (2003) 7724–7732.
- [7] I. Tamm, Y. Wang, E. Sausville, D.A. Scudiero, N. Vigna, T. Oltersdorf, J.C. Reed, IAP-family protein survivin inhibits caspase activity and apoptosis induced by Fas (CD95), Bax, caspases, and anticancer drugs, *Cancer Res.* 58 (1998) 5315–5320.
- [8] S. Gurbuxani, Y. Xu, G. Keerthivasan, A. Wickrema, J.D. Crispino, Differential requirements for survivin in hematopoietic cell development, *Proc. Natl. Acad. U. S. A.* 102 (2005) 11480–11485.
- [9] D.C. Altieri, Targeting survivin in cancer, *Cancer Lett.* 332 (2013) 225–228.
- [10] D.N. Church, D.C. Talbot, Survivin in solid tumors: rationale for development of inhibitors, *Curr. Oncol. Rep.* 14 (2012) 120–128.
- [11] D.C. Altieri, Survivin, cancer networks and pathway-directed drug discovery, *Nat. Rev. Cancer* 8 (2008) 61–70.
- [12] A. Matsuhisa, I. Kinoyama, A. Toyoshima, T. Nakahara, M. Takeuchi, M. Okada, Fused imidazolium derivatives, US Patent 6,734,203 B2, May 11 2004.
- [13] X. Ling, S. Cao, Q. Cheng, J.T. Keefe, Y.M. Rustum, F. Li, A novel small molecule FL118 that selectively inhibits survivin, Mcl-1, XIAP and cIAP1 in a p53-independent manner, shows superior anticancer activity, *PLoS One* 7 (2012) e45571.
- [14] T. Oikawa, Y. Unno, K. Matsuno, J. Sawada, N. Ogo, K. Tanaka, A. Asai, Identification of a small-molecule inhibitor of the interaction between Survivin and Smac/DIABLO, *Biochem. Biophys. Res. Commun.* 393 (2010) 253–258.
- [15] M. Tanioka, H. Nokihara, N. Yamamoto, Y. Yamada, K. Yamada, Y. Goto, T. Fujimoto, R. Sekiguchi, K. Uenaka, S. Callies, T. Tamura, Phase 1 study of LY2181308, an antisense oligonucleotide against survivin, in patients with advanced solid tumors, *Cancer Chemother. Pharmacol.* 68 (2011) 505–511.
- [16] B.D. Cheson, N.L. Bartlett, J.M. Vose, A. Lopez-Hernandez, A.L. Seiz, A.T. Keating, S. Shamsili, K.P. Papadopoulos, A phase II study of the survivin suppressant YM155 in patients with refractory diffuse large B-cell lymphoma, *Cancer* 118 (2012) 3128–3134.
- [17] M.R. Clemens, O.A. Gladkov, E. Gartner, V. Vladimirov, J. Crown, J. Steinberg, F. Jie, A. Keating, Phase II, multicenter, open-label, randomized study of YM155 plus docetaxel as first-line treatment in patients with HER2-negative metastatic breast cancer, *Breast Cancer Res. Treat.* 149 (2015) 171–179.
- [18] N. Nakamura, T. Yamauchi, M. Hiramoto, M. Yuri, M. Naito, M. Takeuchi, K. Yamanaka, A. Kita, T. Nakahara, I. Kinoyama, A. Matsuhisa, N. Kaneko, H. Koutoku, M. Sasamata, H. Yokota, S. Kawabata, K. Furuichi, Interleukin enhancer-binding factor 3/NF110 is a target of YM155, a suppressant of survivin, *Mol. Cell Proteomics* 11 (2012). M111.013243.
- [19] Q. Cheng, X. Ling, A. Haller, T. Nakahara, K. Yamanaka, A. Kita, H. Koutoku, M. Takeuchi, M.G. Brattain, F. Li, Suppression of survivin promoter activity by YM155 involves disruption of Sp1-DNA interaction in the survivin core promoter, *Int. J. Biochem. Mol. Biol.* 3 (2012) 179–197.
- [20] M. Yamauchi, N. Nakamura, M. Hiramoto, M. Yuri, H. Yokota, M. Naitou, M. Takeuchi, K. Yamanaka, A. Kita, T. Nakahara, I. Kinoyama, A. Matsuhisa, N. Kaneko, H. Koutoku, M. Sasamata, M. Kobori, M. Katou, S. Tawara, S. Kawabata, K. Furuichi, Sepantronium Bromide (YM155) induces disruption of the ILF3/p54nrd complex, which is required for survivin expression, *Biochem. Biophys. Res. Commun.* 425 (2012) 711–716.
- [21] A. Rauch, D. Hennig, C. Schäfer, M. Wirth, C. Marx, T. Heinzel, G. Schneider, O.H. Krämer, Survivin and YM155: how faithful is the liaison? *Biochim. Biophys. Acta* 1845 (2014) 202–220.
- [22] H. Tang, H. Shao, C. Yu, J. Hou, Mcl-1 downregulation by YM155 contributes to its synergistic anti-tumor activities with ABT-263, *Biochem. Pharmacol.* 82 (2011) 1066–1072.
- [23] Y.S. Na, S.J. Yang, S.M. Kim, K.A. Jung, J.H. Moon, J.S. Shin, D.H. Yoon, Y.S. Hong, M.H. Ryu, J.L. Lee, J.S. Lee, T.W. Kim, YM155 induces EGFR suppression in pancreatic cancer cells, *PLoS One* 7 (2012) e38625.
- [24] P.C. Lai, S.H. Chen, S.H. Yang, C.C. Cheng, T.H. Chiu, Y.T. Huang, Novel survivin inhibitor YM155 elicits cytotoxicity in glioblastoma cell lines with normal or deficiency DNA-dependent protein kinase activity, *Pediatr. Neonatol.* 53 (2012) 199–204.
- [25] Y.F. Tao, J. Lu, X.J. Du, L.C. Sun, X. Zhao, L. Peng, L. Cao, P.F. Xiao, L. Pang, D. Wu, N. Wang, X. Feng, Y.H. Li, J. Ni, J. Wang, J. Pan, Survivin selective inhibitor YM155 induce apoptosis in SK-NEP-1 Wilms tumor cells, *BMC Cancer* 12 (2012) 619–632.
- [26] T.G. Glaros, L.H. Stockwin, M.E. Mullendore, B. Smith, B.L. Morrison, D.L. Newton, The “survivin suppressants” NSC 80467 and YM155 induce a DNA damage response, *Cancer Chemother. Pharmacol.* 70 (2012) 207–212.
- [27] R.B. Silverman, M.W. Holladay, Chapter 6-DNA-interactive agents, in: R.B. Silverman, M.W. Holladay (Eds.), *The Organic Chemistry of Drug Design and Drug Action*, third ed., Academic Press, Boston, 2014, pp. 275–331.
- [28] G.E. Winter, B. Radic, C. Mayor-Ruiz, V.A. Blomen, C. Trefzer, R.K. Kandasamy, V.K.M. Huber, M. Gridling, D. Chen, T. Klampfl, R. Kralovics, S. Kubicek, O. Fernandez-Capetillo, T.R. Brummelkamp, G. Superti-Furga, The solute carrier SLC35F2 enables YM155-mediated DNA damage toxicity, *Nat. Chem. Biol.* 10 (2014) 768–773.
- [29] A.S. Kalgutkar, I. Gardner, R.S. Obach, C.L. Shaffer, E. Callegari, K.R. Henne, A.E. Mutlib, D.K. Dalvie, J.S. Lee, Y. Nakai, J.P. O'Donnell, J. Boer, S.P. Harriman, A comprehensive listing of bioactivation pathways of organic functional groups, *Curr. Drug. Metab.* 6 (2005) 161–225.
- [30] S.C. Kuo, T. Ibuka, L.J. Huang, J.C. Lien, S.R. Yean, S.C. Huang, D. Lednicer, S. Morris-Natschke, K.H. Lee, Synthesis and cytotoxicity of 1,2-disubstituted naphth[2,3-d]imidazole-4,9-diones and related compounds, *J. Med. Chem.* 39 (1996) 1447–1451.
- [31] G. Giaccone, P. Zatloukal, J. Roubec, K. Floor, J. Musil, M. Kuta, R.J. van Klaveren, S. Chaudhary, A. Gunther, S. Shamsili, Multicenter phase II trial of YM155, a small-molecule suppressor of survivin, in patients with advanced, refractory, non-small-cell lung cancer, *J. Clin. Oncol.* 27 (2009) 4481–4486.
- [32] A. Mahadevan, H. Sard, M. Gonzalez, J.C. McKew, A general method for C3

- reductive alkylation of indoles, *Tetrahedron Lett.* 44 (2003) 4589–4591.
- [33] H. Heaney, S.V. Ley, N-alkylation of indole and pyrroles in dimethyl sulphoxide, *J. Chem. Soc. Perkin Trans. 1* (1973) 499–500.
- [34] L. Gossage, T. Eisen, E.R. Maher, VHL, the story of a tumour suppressor gene, *Nat. Rev. Cancer* 15 (2015) 55–64.
- [35] D.L. Boger, W.C. Tse, Thiazole orange as the fluorescent intercalator in a high resolution fid assay for determining DNA binding affinity and sequence selectivity of small molecules, *Bioorg. Med. Chem.* 9 (2001) 2511–2518.
- [36] W.C. Tse, D.L. Boger, A fluorescent intercalator displacement assay for establishing DNA binding selectivity and affinity, *Acc. Chem. Res.* 37 (2004) 61–69.
- [37] T. Sawahata, R.A. Neal, Biotransformation of phenol to hydroquinone and catechol by rat liver microsomes, *Mol. Pharmacol.* 23 (1983) 453–460.
- [38] T.W. Gant, D.N. Ramakrishna Rao, R.P. Mason, G.M. Cohen, Redox cycling and sulphhydryl arylation; their relative importance in the mechanism of quinone cytotoxicity to isolated hepatocytes, *Chem. Biol. Interact.* 65 (1988) 157–173.
- [39] B. Halliwell, C.E. Cross, Oxygen-derived species: their relation to human disease and environmental stress, *Environ. Health Perspect.* 102 (1994) 5–12.
- [40] P.A. Johnston, K.M. Soares, S.N. Shinde, C.A. Foster, T.Y. Shun, H.K. Takyi, P. Wipf, J.S. Lazo, Development of a 384-well colorimetric assay to quantify hydrogen peroxide generated by the redox cycling of compounds in the presence of reducing agents, *Assay Drug Dev. Technol.* 6 (2008) 505–518.
- [41] W.M. Bonner, C.E. Redon, J.S. Dickey, A.J. Nakamura, O.A. Sedelnikova, S. Solier, Y. Pommier,  $\gamma$ H2AX and cancer, *Nat. Rev. Cancer* 8 (2008) 957–967.
- [42] X. Huang, H.D. Halicka, Z. Darzynkiewicz, Detection of histone H2AX phosphorylation on Ser-139 as an indicator of DNA damage (DNA double-strand breaks), *Curr. Protoc. Cytom.* 30 (2001), 7.27.1–7.27.7.
- [43] E.P. Rogakou, W. Nieves-Neira, C. Boon, Y. Pommier, W.M. Bonner, Initiation of DNA fragmentation during apoptosis induces phosphorylation of H2AX histone at serine 139, *J. Biol. Chem.* 275 (2000) 9390–9395.
- [44] B. Mukherjee, C. Kessinger, J. Kobayashi, B.P.C. Chen, D.J. Chen, A. Chatterjee, S. Burma, DNA-PK phosphorylates histone H2AX during apoptotic DNA fragmentation in mammalian cells, *DNA Repair* 5 (2006) 575–590.
- [45] T. Nakahara, M. Takeuchi, I. Kinoyama, T. Minematsu, K. Shirasuna, A. Matsuhisa, A. Kita, F. Tominaga, K. Yamanaka, M. Kudoh, M. Sasamata, YM155, a novel small-molecule survivin suppressant, induces regression of established human hormone-refractory prostate tumor xenografts, *Cancer Res.* 67 (2007) 8014–8021.
- [46] T. Nakahara, A. Kita, K. Yamanaka, M. Mori, N. Amino, M. Takeuchi, F. Tominaga, I. Kinoyama, A. Matsuhisa, M. Kudoh, M. Sasamata, Broad spectrum and potent antitumor activities of YM155, a novel small-molecule survivin suppressant, in a wide variety of human cancer cell lines and xenograft models, *Cancer Sci.* 102 (2011) 614–621.
- [47] C. Lu, F. Zhu, Y.Y. Cho, F. Tang, T. Zykova, W.Y. Ma, A.M. Bode, Z. Dong, Cell apoptosis: requirement of H2AX in DNA ladder formation, but not for the activation of caspase-3, *Mol. Cell.* 23 (2006) 121–132.
- [48] Y.J. Zhang, C.R. Lu, Y. Cao, Y. Luo, R.F. Bao, S. Yan, M. Xue, F. Zhu, Z. Wang, L.N. Duan, Imatinib induces H2AX phosphorylation and apoptosis in chronic myelogenous leukemia cells in vitro via caspase-3/Mst1 pathway, *Acta Pharmacol. Sin.* 33 (2012) 551–557.
- [49] S. Solier, Y. Pommier, The apoptotic ring: a novel entity with phosphorylated histones H2AX and H2B and activated DNA damage response kinases, *Cell Cycle* 8 (2009) 1853–1859.
- [50] K.M. Soares, N. Blackmon, T.Y. Shun, S.N. Shinde, H.K. Takyi, P. Wipf, J.S. Lazo, P.A. Johnston, Profiling the NIH Small Molecule Repository for compounds that generate H2O2 by redox cycling in reducing environments, *Assay Drug Dev. Technol.* 8 (2010) 152–174.
- [51] R.A. Irizarry, B. Hobbs, F. Collin, Y.D. Beazer-Barclay, K.J. Antonellis, U. Scherf, T.P. Speed, Exploration, normalization, and summaries of high density oligonucleotide array probe level data, *Biostatistics* 4 (2003) 249–264.